Title
Mechanisms of Ras Signaling and Activation on Reconstituted Membrane Surfaces

Author
Lam, Hiu Yue Monatrice

Publication Date
2017

Peer reviewed|Thesis/dissertation

Mechanisms of Ras Signaling and Activation on Reconstituted Membrane Surfaces

by

Hiu Yue Monatrice Lam

A dissertation submitted in partial satisfaction of the

requirements for the degree of

Doctor of Philosophy

in

Chemistry

in the

Graduate Division

of the

University of California, Berkeley

Committee in charge:

Professor Jay T. Groves, Chair
Professor John Kuriyan
Professor James H. Hurley

Spring 2017

Abstract

Mechanisms of Ras Signaling and Activation on Reconstituted Membrane Surfaces
by
Hiu Yue Monatrice Lam

Doctor of Philosophy in Chemistry
University of California, Berkeley
Professor Jay T. Groves, Chair

The membrane is a crucial component of the cell that modulates protein spatial organization and enzyme-substrate reactions, which, in turn, mediates cellular signal transmission. One key membrane protein is the small GTPase Ras, which acts as a signaling node that determines cellular outcome. Though Ras is an attractive target for anticancer therapies, effective treatments against its oncogenic mutants remain elusive due to the incomplete understanding of its signaling potential in the membrane environment. Here, we seek to elucidate some of the key biophysical properties and regulations of Ras on membranes in reconstituted systems.

Lateral organization, especially dimerization, of Ras on cellular membranes has long been a subject of great interest. We find that Ras dimers can form on membranes by photosensitization reactions, in which molecular oxygen mediates protein radicalization under typical fluorescence experimental conditions. Inter-protein dityrosine crosslinking is one of the dimerization motifs, and the specific surface tyrosine distribution on Ras renders the protein especially sensitive to this reaction. Photosensitization reactions are reflective of physiological oxidative stress induced by reactive oxygen species, suggesting such processes may occur naturally in cells.

Ras activation is a critical step for receptor tyrosine kinase signal transduction. One key activator of Ras is the enzyme Son of Sevenless (SOS), which catalyzes Ras nucleotide exchange. The complex domain architecture of SOS ensures efficient Ras turnover only when all activation inputs are met, including stable membrane recruitment. Notably, a single molecule of SOS can processively turnover thousands of Ras molecules upon allosteric Ras engagement, and generation of Ras.GTP creates positive feedback by enhancing SOS recruitment. We developed a real-time Ras activation assay to detect the activity of purified, full-length SOS (SOS^{FL}) molecules exposed to inactive Ras on membranes. Despite the collective autoinhibition from the N- and C-terminal domains of the enzyme, SOS^{FL} is nonetheless capable of inducing rapid Ras activation by single proteins. Our measurements further reveal a new mechanism of Ras.GTP-mediated SOS activation through enhancement in probability of single SOS to transition to the hyperactive state. Processively active single SOS molecules are thus consequential in Ras signaling and additional measures are necessary to suppress spurious Ras activation.

To my parents

Table of Contents

Acknowledgements iii

1. Introduction
- 1.1 The significance of the membrane in signal transduction 1
- 1.2 Ras as the subject of interest 2
- 1.3 Regulation of Ras and other G-proteins 2
- 1.4 Signaling upstream of Ras 4
- 1.5 Signaling downstream of Ras 5
- 1.6 Oncogenic Ras mutations 5
- 1.7 Supported membrane platform 6
- 1.8 Research focus 7

2. Covalent Ras dimerization on membrane surfaces through photosensitized oxidation
- 2.1 Introduction 9
- 2.2 Results 11
- 2.3 Discussion 18
- 2.4 Materials and methods 19

3. Primary mode of SOS catalysis is through processive Ras activation by single proteins
- 3.1 Introduction 23
- 3.2 Results 26
- 3.3 Discussion 36
- 3.4 Materials and methods 39

4. Conclusions
- 4.1 Summary of findings 44
- 4.2 Future directions 44

5. References 48

Acknowledgments

I would like to thank my family, friends, and mentors for their tremendous support on my graduate school journey. My parents and grandparents have always emphasized the importance of education, and I am privileged to have the opportunity to attend college and graduate school in the United States. They worked hard and made sacrifices so that I can pursue higher education. I am thankful for my friends at Berkeley, who made the grueling process of graduate school much more enjoyable. My friends from Hong Kong and Washington University have been generous with their time whenever I have the chance to visit, and help me feel more invigorated in my research by giving me a wider perspective.

My advisor, Jay Groves, has been encouraging throughout my time in the lab and taught me how to think critically and analytically while keeping the big picture in mind. I am very appreciative of the freedom he gives to his students to work on various projects, and for fostering a collaborative environment where lab members can learn from one another. His ability to create a compelling story from seemingly disjointed pieces of work is one that I strive to emulate.

I would like to thank former and current members of the Groves lab for being so incredibly welcoming and delightful to work with. They have taught me a great deal, from operating lab instruments to thinking about scientific problems from multiple angles. I would like to give a special mention to the following members: Dr. Hsiung-Lin Tu, Dr. Sune Christensen, Dr. Wan-Chen Lin, Dr. Nicole Fay, Dr. Kate Alfieri, Dr. Hector Huang, Dr. Geoff O'Donoghue, Dr. Rafal Pielak, Dr. Tomas Laursen, Dr. Jean Chung, Dr. Young Kwang Lee, Dr. Scott Hansen, Dr. William Huang, Dr. Shalini Low-Nam, and Jenny Lin. I would like to give a special shout-out to Steven Alvarez, who has been my wingman inside and outside of lab.

Last but not least, I would like to thank my former mentors from secondary and undergraduate school for their advice and teachings for me to become who I am today.

1. Introduction

The significance of the membrane in signal transduction

Signal transduction occurs when particular inputs trigger a series of chemical reactions, which ultimately lead to cellular decision making. Though many important insights on signaling are generated by mapping protein-protein interactions to phenotypic outcomes, a key element is often omitted—the membrane. If thought simplistically, the membrane physically separates cellular components from the external environment, thus controlling transport of matter across the cell while preventing the two parts from reaching chemical equilibrium. However, membranes are not just passive barriers. Instead, they have unique physical properties to modulate protein spatial organization and signal transmission (1).

The plasma membrane (PM) constitutes a diverse set of lipids and proteins, which vary greatly in composition across space and time (2). It presents many functional groups for protein attachment and stabilization of structural conformations suited for signal propagation. Protein recruitment to a two-dimensional surface from solution also increases its local concentration and, thus, facilitates signal amplification (3, 4). The PM interestingly displays large-scale composition fluctuations that indicate it is close to the miscibility critical point under physiological conditions (5, 6). Therefore, it is capable of undergoing macroscopic phase transitions with little to no energy input, providing a platform for rapid rearrangement of signaling domains.

The connection between the PM and the actin cytoskeleton provides another dimension where the membrane directly mediates protein binding kinetics, spatial organization, and signaling (7). For example, T cells trigger an immune response upon interactions with antigen presenting cells (APCs). This requires T cell receptor (TCR) engagement with peptide major histocompatibility complex (pMHC) ligands followed by cytoskeleton-mediated clustering of TCR:pMHC and adhesion molecules to form the immunological synapse (8-10). TCR:pMHC association and dissociation kinetics are greater on cell membranes than in solution by orders of magnitude, indicating that the membrane environment is critical for T cell responsiveness by controlling ligand sampling frequencies (11, 12). TCR:pMHC cluster formation also pins the membrane over micrometer-sized areas such that larger CD45 phosphatases are physically segregated from the central supramolecular activation cluster (cSMAC), enabling sustained downstream signaling from activated TCRs (13).

In addition, the PM constantly interacts with the extracellular microenvironment, suggesting it can relay external signals to inside the cell through mechanical force sensing (14). The mechanisms are still being explored, but the ability for the PM to sense and transmit signals from the external environment is shown in cell studies where bulky polymers in the glycocalyx affect integrin assembly on the PM and increase cell survival (15).

Ras as the subject of interest

Many proteins vital to cellular function are associated with the membrane, but one membrane protein, in particular, continues to stump scientists ever since its discovery in the 1960s (16, 17). It is the ubiquitously expressed protein Ras, which, once activated, can interact with a multitude of downstream effector proteins and determine cellular outcomes, such as cell proliferation and survival (18, 19). Ras has been studied intensely over multiple decades because 20% of all human tumors harbor its mutations and yet, there is no effective treatment against Ras-related diseases to date (20). Drugging Ras is challenging due to its picomolar affinity for nucleotides and the lack of well-defined features for small molecules to bind (21). While there is ongoing research on Ras direct inhibitors, efforts have shifted to find indirect targets, for example through disruptions in downstream effector protein interactions and Ras-regulated metabolic pathways (22). A tremendous amount about Ras signaling has been revealed in the last 40 years, but it is clear that many mysteries remain unsolved.

Regulation of Ras and other G-proteins

Ras is the founding member of small guanine nucleotide-binding (G) proteins, or small GTPases, which consists of over 150 proteins with masses typically in the range of 20-25 kDa (23). They are comprised of a G-domain, which contains conserved N/TKXD and GXXXXGKS/T (P-loop) motifs that bind guanine nucleotides, and flanking residues that are posttranslationally modified and serve as membrane localization signals (24, 25). For example, Ras has four isoforms (H-Ras, N-Ras, K-Ras-4A, and K-Ras-4B) and each consists of a

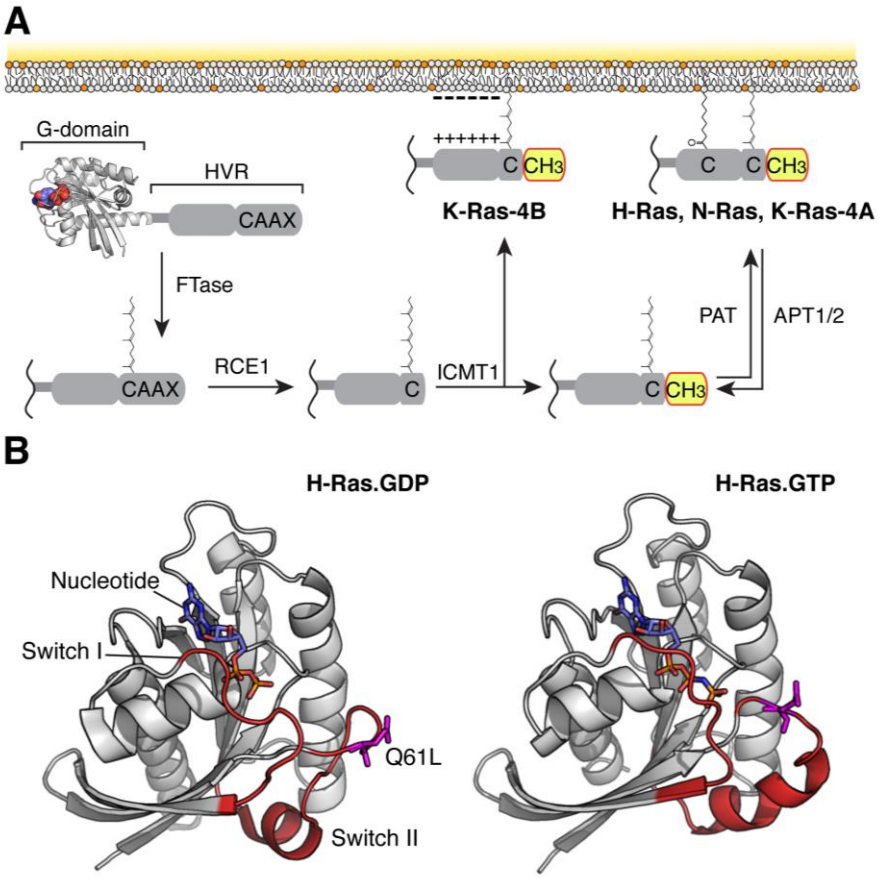

Figure 1-1. Variations in the Ras G-domain and HVR. (A) Posttranslational modifications of the HVR and lipid anchoring of the four Ras isoforms. (B) Nucleotide-dependent structural variations in Ras G-domain. PDB codes: 1Q21 (Ras.GDP) and 5P21 (Ras.GNP).

distinct set of lipid tails and amino acids in the C-terminal hypervariable region (HVR) that govern their cellular localization and compartmentalization. (**Fig. 1-1A**) (25-27). Small GTPases are aptly refereed to as "molecular switches" as they have two distinct states: a GDP-bound inactive state and an active GTP-bound state (24). The switch 1 and 2 regions of the G-domain undergo pronounced structural changes when the bound nucleotide changes identity, for example from GDP to GTP, and does the orientation of the G-domain on the membrane (**Fig. 1-1B**) (26, 28). Only in the active form can small GTPases interact with effector proteins to propagate signals downstream to cause a cellular response.

Small GTPases are intrinsically inefficient signal transducers. They bind to guanine nucleotides with nanomolar to picomolar affinity, so bound-nucleotides dissociate on the order of hours (29). At the same time, these proteins have inherently low GTP hydrolysis activity, meaning that they remain active for long periods once bound to GTP. However, there are various enzymes to regulate their activation and deactivation. Guanine nucleotide exchange factors (GEFs) catalyze small GTPase activation by binding and perturbing the structure of the G-domain, which weakens its affinity to the bound nucleotide (**Fig. 1-2A**) (29). After nucleotide displacement, small GTPase binding to GTP is favored over GDP due to the ten-fold greater concentration of GTP to GDP in the cell, which subsequently puts the protein in the active state. On the other hand, GTPase-activating proteins (GAPs) accelerate GTP hydrolysis by stabilizing the transition state of the reaction and coordinating a water molecule to the γ-phosphate of the bound-GTP typically through an arginine finger (**Fig. 1-2B,C**) (29). The collective mechanisms of GEFs and GAPs thus provide critical regulation for small GTPases to integrate input signals efficiently and to produce cellular outcome with high fidelity.

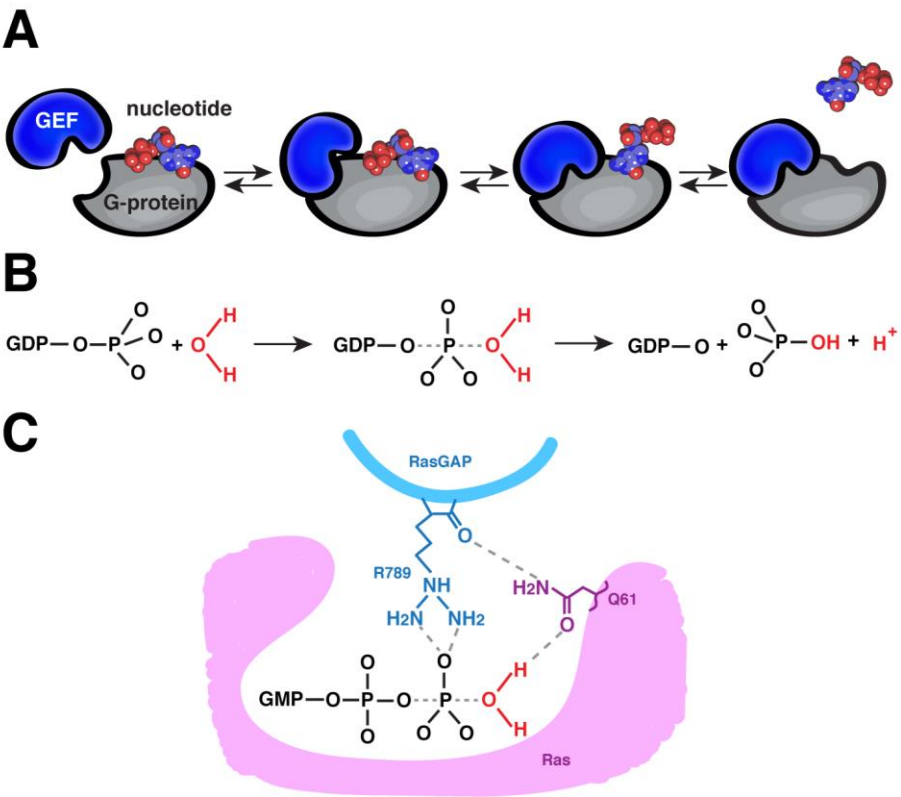

Figure 1-2. General mechanisms of small GTPase regulation. (A) Mechanism of GEF-catalyzed nucleotide exchange on G-proteins. (B) Chemical equation of GTP hydrolysis. (C) Schematic of GTP hydrolysis in the Ras active site enabled by RasGAP through coordination with the arginine finger (R789).

Signaling upstream of Ras

The widely accepted pathway of Ras activation starts with receptor tyrosine kinase (RTK) stimulation by growth factors (**Fig. 1-3A**) (30, 31). Tyrosine residues in the cytoplasmic domains of RTK become phosphorylated, which lead to the recruitment of the adaptor proteins Grb2 via SH2-domain binding. Son of Sevenless (SOS), a ubiquitously expressed GEF, is then recruited to the PM by binding the Grb2 SH3 domains via its proline-rich (PR) domain at the C-terminus (32-34). Membrane-bound SOS can subsequently bind and activate Ras on the PM to propagate input signals downstream.

However, there are many additional layers of complexity that govern SOS-catalyzed Ras activation. SOS is autoinhibited in the cytosol by the histone fold, Dbl-homology, and Pleckstrin-homology domains at the N-terminus as well as the C-terminal PR domain (35, 36). Autoinhibition is relieved when these regulatory domains interact with lipids or proteins on membrane surfaces. The Ras binding sites of SOS at the catalytic core (SOS^{cat}) can subsequently interact with membrane-bound Ras and catalyze nucleotide exchange (**Fig. 1-3B**) (35, 37-39). SOS contains two Ras-binding sites: a catalytic pocket where nucleotide exchange is performed, and an allosteric pocket that causes a ten-fold increase in catalytic rate when bound to Ras.GTP compared to Ras.GDP (38). This key feature of SOS^{cat} constitutes the positive feedback loop. Membrane interactions are also critical for SOS catalysis as the nucleotide exchange rate of SOS^{cat} on membranes is 500-fold greater than that in

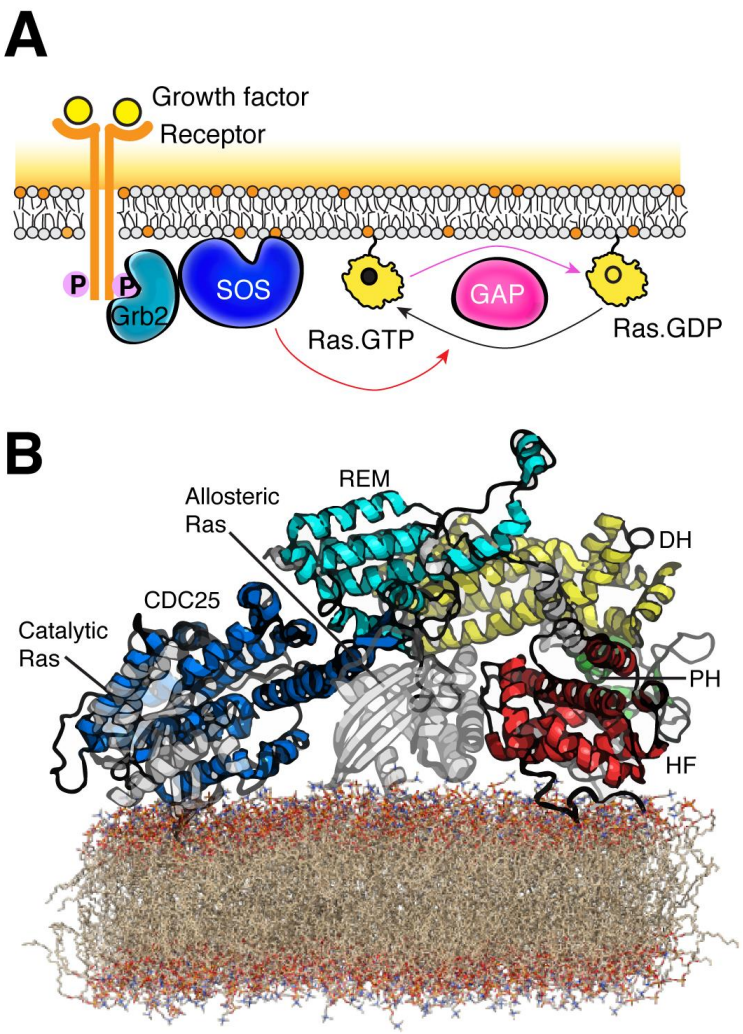

Figure 1-3. General mechanism of Ras activation by SOS. (A) Conventional pathway of Ras activation induced by RTK stimulation. (B) Schematic of SOS with a truncated PR-domain bound to two Ras molecules (gray) on membranes to catalyze nucleotide exchange. PDB codes: 3KSY (SOS 1-1049) and 1XD2 (Ras molecules).

solution (40). While many structural and cell studies have provided great insight on SOS function, there are many additional questions that have yet to be addressed (see Research Focus).

Signaling downstream of Ras

Upon activation, Ras can bind to a multitude of effector proteins, which generates particular cellular responses (30). There are four known effector proteins of Ras to date: Rapidly Accelerated Fibrosarcoma (Raf), phosphatidylinositol-3-kinase (PI3K), Ral guanine nucleotide dissociation stimulator (RalGDS), and phospholipase C-epsilon (PLCε). The Ras binding domain (RBD) of the effector proteins have similar structures though the amino acid sequences are not conserved (41). Ras engagement causes conformational changes in effector proteins and stabilizes them on membrane surfaces. This positions the proteins to be in proximity with binding partners and facilitates reactions that lead to their full activation (30). One example is that Ras binding relieves Raf autoinhibition and, in turn, the kinases SFKs and CK2 can access and phosphorylate specific residues to activate Raf (42). Proteins downstream of Ras directly modulate a broad range of cellular reactions, such as lipid phosphorylation, calcium mobilization, and activation of various kinases, transcription factors, and small GTPases (30). Given the ability for Ras to trigger such a vast number of cellular processes, it is critical that Ras is not aberrantly activated.

Oncogenic Ras mutations

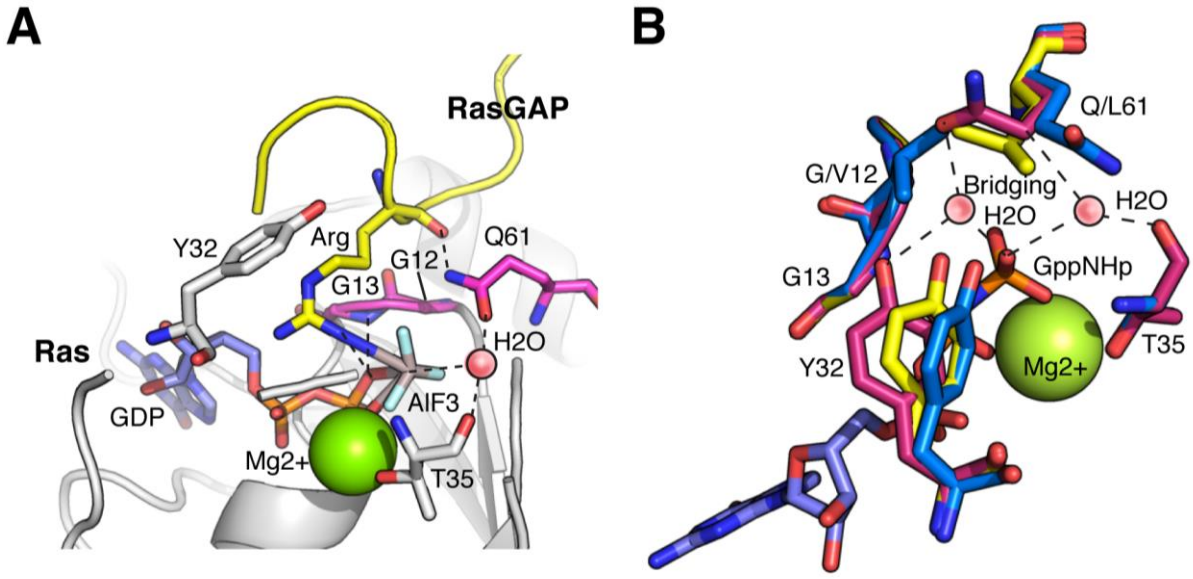

Figure 1-4. Structural effects of oncogenic Ras mutants. (A) Nucleotide binding site of Ras that is in complex with RasGAP. The arginine finger (Arg 789) is inserted into the Ras active site. (B) Structural changes in the Ras active site with oncogenic mutations present at G12 and Q61 residues. Hydrogen bonds between residues and water molecules are depicted as dashed lines. PDB codes: 1WQ1 (RasGAP with Ras), 3K8Y (Ras WT), 3OIW (Ras G12V), and 3OIU (Ras Q61L).

Mutations that deregulate the cycle of Ras activation and deactivation can lead to fatal consequences. Three oncogenic Ras mutations, specifically at codons 12, 13, and 61, reduce the effectiveness of intrinsic as well as GAP-catalyzed GTP hydrolysis, which put Ras in the constitutively active state (43). Augmented Ras activation subsequently causes hyperactivation or overexpression of various cellular components and turn healthy cells cancerous. Structural studies show that mutations at G12 and G13 residues to bulky amino acids sterically hinder the GAP arginine finger from stabilizing the transition state for accelerated GTP hydrolysis (**Fig. 1-4A**) (43). The Q61 residue plays a key role in coordinating a water molecule and positioning the GAP arginine finger in the Ras active site via its carbonyl and amide side chains (**Fig. 1-2B**, **Fig. 1-4B**) (43). Therefore, Q61 mutations inhibit the transition state of GAP-assisted GTP hydrolysis to form though GAP binding is unaffected (43). In addition, it has been demonstrated that mutations at G12 and Q61 reduce Ras intrinsic GTPase activity by displacing a bridging water molecule that stabilizes charges in the active site during GTP hydrolysis (**Fig. 1-4B**) (43).

The outcome of oncogenic Ras mutations is dependent on both the tissue context and the Ras isoform that is mutated. K-Ras is the most frequently mutated Ras isoform found in tumors of endodermally derived tissues, such as lung, pancreas, and colon (30, 43). However, the exact mechanism that leads to isoform-specific phenotypes is still unclear. Studies suggest that Ras isoforms differentially trigger signaling downstream pathways due to more potent activation of certain effector proteins (44-46). For example, a G12V point mutation in K-Ras prevents differentiation and promotes proliferation in endodermal progenitor cells whereas the same mutation in H-Ras increases differentiation and growth arrest (47). On the other hand, the N-Ras G12V mutant causes no observable effect (47). There are additional questions regarding Ras oncogenic mutants that remain unanswered. For example, it is not well understood why mutations at codons 12, 13, or 61 occur at variable frequencies (48). It is also unclear why certain point mutations, such as G12V and Q61L, are more prevalent in cancer than others (43). Recent and future advances in technology and research tools will likely help progress our understanding on how specific Ras mutations lead to cancer development in an isoform-dependent manner.

Supported membrane platform

One main reason Ras is incompletely understood is due to the technical difficulties of studying it in the membrane context. Ras studied *in vitro* were primarily performed in solution despite early discoveries that showed membrane association is necessary for Ras function (49). Solution measurements provided great structural and mechanistic insights into Ras regulation and signal transduction (50-53), but many properties of Ras were only recently revealed when protein-membrane interactions were considered, such as Ras spatiotemporal organization (54-56) and nanoclustering (57, 58). These findings, determined using cell-based assays, contributed to our understanding on how Ras behaves under physiological conditions. However, it is difficult to assign observed behavior to specific mechanisms due to the complexities and interdependencies that exist in cells.

In order to quantitatively map out the input-outcome response that govern Ras signaling, it is important to study Ras under rigorously controlled systems while permitting protein-membrane interactions. For this reason, we adopt a reductionist's approach to study Ras reconstituted on supported membranes (39, 59). The supported lipid bilayer (SLB) platform allows precise control of the membrane composition and provides a planar geometry compatible with fluorescence microscopy and spectroscopy techniques (60). A major advantage of this system is that the membrane is fluid, which preserves the lateral mobility of lipids and membrane-tethered proteins in cellular membranes so that their spatial organization can be characterized. Though it is possible to create SLBs using a wide range of lipids to attempt to mimic native membranes, it is easy to lose sight of how each component affects the physical properties of the membrane. Thus, we use simple lipid mixtures to create highly fluid bilayers, which allow proteins of interest to be characterized quantitatively in the membrane environment without being belabored by possible complexities due to lipid composition.

Research focus

The SLB platform allows us to gain mechanistic insights on Ras signaling in the membrane environment using quantitative measurements. There are many outstanding questions in the field and this dissertation focuses on addressing two areas: (1) Ras spatial organization, specifically dimerization, and (2) Ras activation by single SOS molecules on membranes.

Research in the past two decades has shed light on the extensive spatiotemporal organization of Ras in cells (43). It was first hypothesized that Ras dimerizes and functions as a dimeric unit about 20 years ago (61), which supports findings that its downstream effector protein Raf dimerizes in the process of activation (62, 63). Although recent *in vitro*, *in silico*, and cell studies show that Ras can form dimers on membranes and in solution (59, 64-66), it remains controversial if Ras has the intrinsic properties to dimerize (67). Ras dimers have been observed in crystal structures (68), but it is unclear if they exist under physiological densities in the membrane context. If there exists a Ras dimer interface, it would present a new regulatory mechanism for Ras activation and possibly a druggable target. The first part of my dissertation addresses this question and offers insight on Ras covalent dimerization driven by photosensitized oxidative reactions in the absence of binding partners.

Another underexplored area in Ras signaling is the capability and significance of Ras activation by single molecules of SOS with its complete domain architecture. SOS is a tightly autoregulated protein that has two Ras binding sites at the catalytic core with flanking regulatory domains (**Fig. 1-3B**) (34, 36-38). The catalytic core creates a positive feedback loop where active Ras binding at the allosteric pocket leads to increased Ras activation via two mechanisms: increased Ras turnover activity at the catalytic pocket (38, 69), and augmented SOS recruitment to the membrane (36, 70). Recent work looking at single molecules of SOS in reconstituted systems revealed that dual Ras binding stably anchors SOS to membranes, enabling turnover of thousands of Ras molecules over minutes by a single enzyme (39, 70, 71). This processive behavior of SOS is kept in check by the N- and

C-terminal domains, which independently inhibit Ras binding at the allosteric site (36, 71, 72). However, it is unclear if full-length SOS domain architecture can access the processive activation state if it was initially autoinhibited without receptor-mediated membrane-recruitment. In addition, the range of activity states achievable by full-length SOS and their significance in Ras signaling remain unknown. The second part of the dissertation addresses these questions and provides an understanding on the capability of single SOS molecules to activate Ras in spite of opposition from autoinhibition and Ras deactivation activity.

2. Covalent Ras Dimerization on Membrane Surfaces through Photosensitized Oxidation[1]

Introduction

Ras is a critical protein that serves as a molecular switch in cellular signaling, cycling between GDP- and GTP-bound states on membranes as a part of many signaling pathways (73). Its importance is underscored by the fact that its oncogenic mutants are found in 30% of human cancers (74, 75). As with many other membrane-bound signaling proteins, the lateral organization of Ras on membrane surfaces such as dimerization, clustering, and partitioning into different membrane regions are thought to be an integral part of Ras signal regulation (76, 77). Manipulation of the lateral organization of Ras has also emerged as an alternative strategy for anticancer therapies, since traditional small-molecule approaches to directly inhibit Ras have been largely unsuccessful to date (78-81). Dimerization of Ras has been predicted based on its structure (82) as well as interactions with regulators and effectors (e.g. Raf kinase and SOS) in the cellular context (39, 40), but the intrinsic potential of Ras to form molecular dimers on membranes or its effect on signaling in cells remain unclear.

Ras dimers have been detected using optical techniques such as superresolution microscopy, dynamic light scattering (DLS), Förster resonant energy transfer (FRET), fluorescence correlation spectroscopy (FCS), photon counting histogram (PCH), and single particle tracking (SPT) (66, 82-84). While these methods identify the presence of Ras dimers and clusters, the identity of the dimeric or clustered species has not been revealed. Through efforts to determine the dimerization kinetics of Ras on membranes using fluorescence methods, we have found that Ras exhibits a distinctively high potential to form covalent dimers through oxidative reactions. A clue came from single particle tracking experiments that followed long trajectories of single Ras molecules diffusing on the membrane. Dimer association or dissociation events were never observed in trajectories lasting up to several seconds (**Fig. 2-1**). As fast kinetics would typically be expected for a weak dimerization interaction, this suggested that Ras dimers were not in dynamic equilibrium with the monomeric species; rather, the slow kinetics were more consistent with permanently crosslinked products. Fluorescence spectroscopy further reveals covalent dityrosine formation as one of the dimerization motifs, which may explain why Ras dimerization exhibits sensitivity to the mutation of protein surface tyrosine residues. Although such oxidative reactions on proteins are well known (85), the high reactivity and sequence specificity exhibited by Ras in comparison to other proteins appear to be unappreciated aspects in the multifaceted behavior of this protein. Such reactions could be produced in a physiological setting by oxidative stress induced by reactive oxygen species (ROS) (86). More broadly, visible light photoredox reactions have emerged in recent years as a chemical mechanism with applications in catalysis and small molecule activation (87).

[1] This chapter is from the published work in J. K. Chung*, Y. K. Lee*, H. Y. M. Lam*, and J. T. Groves. *JACS,* **2016**, *138* (6), pp 1800-1803. * denotes equal contributions.

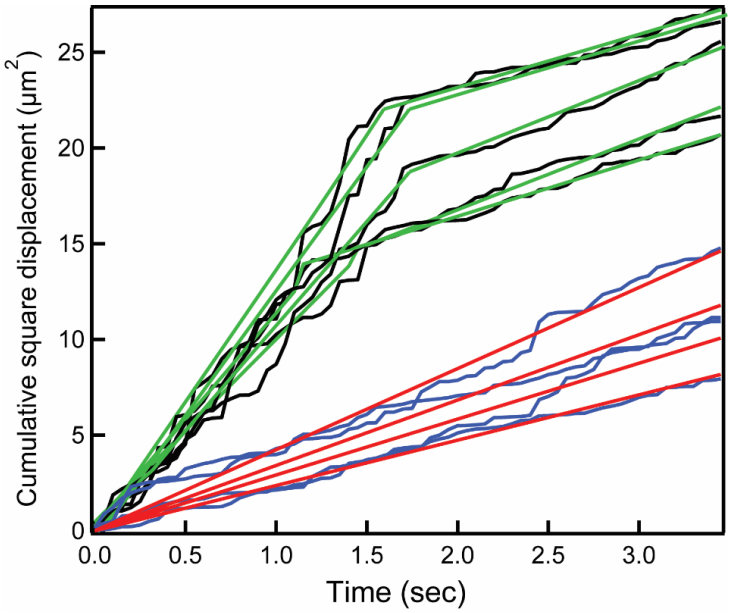

Figure 2-1. Long trajectories of Ras on SLB by SPT. Cumulative square displacement plots (CSD) of individual wild type H-Ras trajectories (blue line). The plots well agree with linear fit- ting (red line), showing Ras stay in a single diffusion state until they bleach out. Simulated trajectories undergoing diffusion coefficient change from 3 to 0.7 $\mu m^2/s$ exhibit change points of diffusion sate (black line: CSD of simulated trajectories; green line: linear fitting of CSD). Change points were detected by Bayesian detection model.

Results

To quantitatively characterize the extent of Ras dimerization on membranes, Ras was reconstituted *in vitro* on a supported lipid bilayer (SLB) (**Fig. 2-2**). The SLB platform mirrors the cellular membrane environment while providing a planar geometry amenable for quantitative fluorescence experiments (60, 88). In this setup, Ras was coupled to the membrane via a maleimide-thiol reaction between the terminal cysteine (C181) and the headgroup of MCC-DOPE lipid. Fluorescently labeled nucleotide ATTO 488-GDP or ATTO 488-GppNHp were used to track the protein. When Ras dimerizes, it diffuses significantly more slowly, as the diffusion coefficient for doubly anchored species is appreciably lower than that for singly anchored species on an SLB (89, 90). The mobility of Ras on the surface monitored by both FCS and SPT shows an increasing fraction of a slower-diffusing population as the overall Ras density on the membrane increases, indicating a higher fraction of Ras dimers.

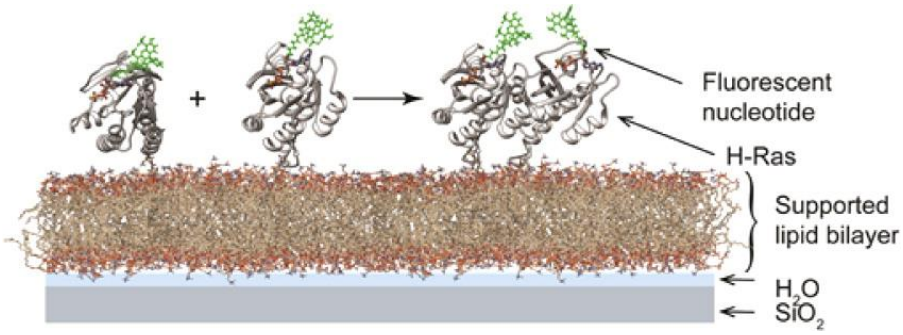

Figure 2-2. Experimental schematic of reconstituted Ras on a supported lipid bilayer (structure from PDB ID 4EFL). The globular domain of Ras was covalently bound to the bilayer, and fluorescently labeled nucleotides were used to track Ras.

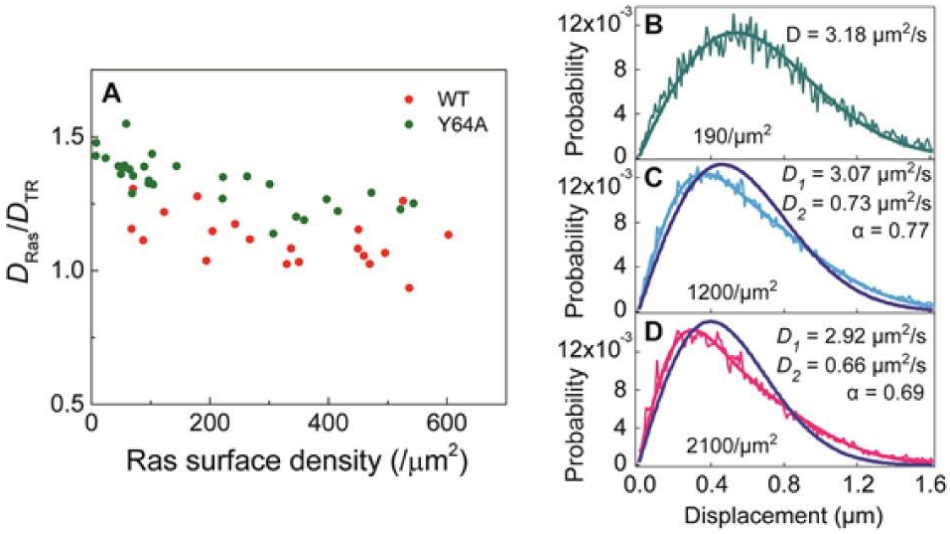

Figure 2-3. Density-dependent diffusion of H-Ras on SLB. (A) Relative diffusion of fully labeled Ras compared to fluorescent lipids (Texas Red-DHPE, TR) measured by FCS shows apparent decrease with increasing Ras surface density. (B–D) Step-size distribution of fully labeled wild-type Ras at low (B), medium (C), and high surface densities (D). For (B), the data were fit to the single-species Brownian diffusion model, and (C) and (D) were fit to two-species model to extract diffusion coefficients of the fast species ($D1$) and the slow species ($D2$), and the fraction of fast species (α). The blue lines represent ill-fitting single-species model.

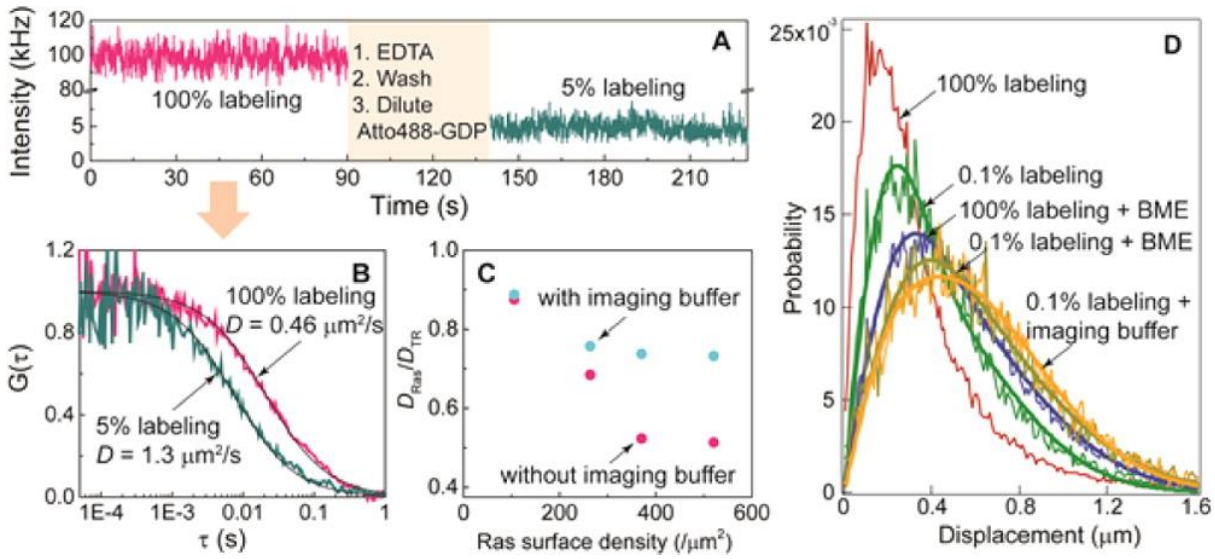

Figure 2-4. Photosensitized crosslinking of H-Ras on membranes. (A) Fluorescence intensity fluctuation of a high-density His6-Ras sample (~1600/μm²) in an underlabeling experiment. Initially, the sample is fully labeled (magenta trace). Then, the sample is washed and underlabeled (green trace). (B) Autocorrelation of intensity fluctuations. (C) Diffusion coefficients of fully labeled His6-Ras samples with (blue) and without imaging buffer (magenta) measured by FCS. (D) Step-size distributions of high density Ras (~4500/μm²) under the various imaging conditions.

Figure 2-3A shows overall decreasing diffusion measured by FCS with increased surface density for the wild type and Y64A mutant H-Ras, although the extent of the effect differs between the constructs. We also observe a similar density-dependence in diffusion in SPT (**Fig. 2-3B-D**). At low surface densities (**Fig. 2-3B**), the step size distribution acquired from wild type Ras diffusion trajectories is adequately described by the two-dimensional, single-species Brownian diffusion model. However, the analysis of these step size distributions at higher surface densities confirms the presence of a second, more slowly diffusing species (**Fig. 2-3C, D**). The relative fraction of slow diffusing species increases as the overall Ras surface density increases, while the diffusion coefficients of both fast and slow species remain constant. These results indicate a surface concentration-dependent dimerization, and resemble a two-dimensional equilibrium dimerization reaction (84). However, in efforts to characterize the dynamic dimerization equilibrium by measuring the Ras dimer kinetic lifetime, we found evidence for long-lived species that were more suggestive of a non-equilibrium state and covalent dimers (**Fig. 2-1**).

We hypothesized covalent crosslinking driven by oxidative stress, specifically by fluorophore-mediated photosensitization in this case, was involved in the Ras dimer formation. To test this hypothesis, two conditions expected to reduce these oxidative effects were tested: (1) reducing the total number of fluorescent molecules in the system by substoichiometric labeling (where only a small fraction Ras is bound to fluorescent nucleotides, and the rest to dark, native nucleotides), and (2) using an enzymatic oxygen scavenging imaging buffer (IB) cocktail. **Figure 2-4A, B** show the effect of under-labeling in FCS by comparing the mobility of fully labeled Ras (magenta traces) and at 5% labeling

(green traces). For the same sample, underlabeling not only proportionately decreases the average intensity of fluorescence (**Fig. 2-4A**), but also substantially increases the diffusion coefficient of Ras (**Fig. 2-4B**). Similarly, when an IB composed of Trolox, glucose oxidase, catalase, and β-mercaptoethanol (BME) is used instead of plain HEPES buffer during FCS data acquisition, Ras shows faster diffusion at the same densities, although IB does not completely eliminate the reduction in mobility (**Fig. 2-4C**).

The results from analogous SPT experiments are consistent with the FCS observations. At a very high Ras surface density (~4500/μm^2, **Fig. 2-4D**), the step size distribution of fully labeled Ras shows complex diffusion behavior that requires a diffusion model with more than two species (**Fig. 2-4D** red curve). The addition of BME significantly alleviates the slowing of diffusion, as thiols not only serve as a reducing agent but also as a singlet oxygen quencher, thus mitigating molecular oxygen-mediated crosslinking (91, 92). However, substantial crosslinking occurs in SPT even at an extremely underlabeled condition (0.1% labeling, **Fig. 2-4D** green curve).

The SPT underlabeling experiment reveals important mechanistic aspects of the oxidative crosslinking. Considering the duration of an SPT experiment and the diffusion rate of Ras on SLB, it is unlikely that a labeled protein will encounter another labeled protein at 0.1% labeling. Crosslinking in spite of such low collision probability between labeled proteins suggests that it involves a catalytic intermediate rather than occurring through direct dye-dye interactions. This is consistent with Type II photosensitized reaction, in which the photosensitizer, such as fluorescent dye, is quenched from the triplet state (T_1) to ground state (S_0) by molecular oxygen. The oxygen then becomes excited to the singlet electronic state ($^1O_2$), a highly unstable and reactive species that may react with the protein of interest, resulting in structural changes such as fragmentation, dimerization, aggregation, or denaturation (93). The aromatic amino acids tyrosine, histidine and tryptophan, as well as sulfur-containing methionine and cysteine are especially vulnerable to oxidative reactions (93, 94). A single dye molecule could visit the excited triplet state and relax back to the ground state multiple times, catalytically producing one singlet oxygen molecule in each cycle, until the dye is eventually irreversibly oxidized (95). This mechanism is illustrated in **Figure 2-5**.

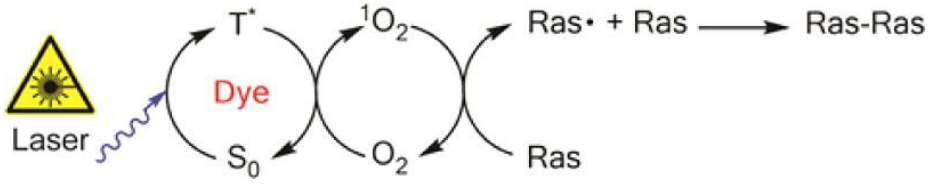

Figure 2-5. Type II photosensitization crosslinking of Ras. Proposed mechanism of nonspecific crosslinking reaction involves the dye photosensitizer cycling between the ground (S_0) and triplet states (T*). The energy transfers to molecular oxygen (O_2), which becomes excited to the singlet state ($^1O_2$). This ROS reacts with Ras, which forms a free radical species and crosslinks with another Ras.

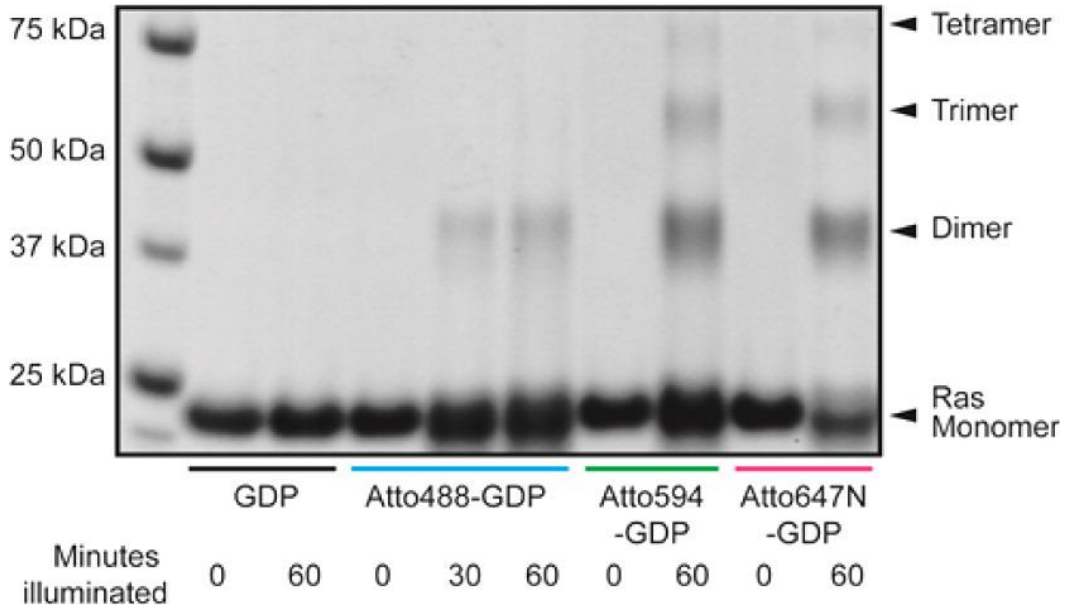

Figure 2-6. SDS-PAGE gel electrophoresis of laser-irradiated H-Ras. In the presence of GDP labeled with various photosensitizers, Ras forms covalent dimers and higher-order oligomers.

In order to confirm the formation of Ras covalent dimers through oxidative reactions, the globular part of H-Ras (21 kDa) was irradiated in the presence of different sensitizers (GDP labeled with ATTO series dyes: 488, 594, and 647N) in solution with cw diode laser sources at appropriate wavelengths (485 nm, 561 nm, 640 nm). The irradiance for this experiment was kept near 0.03 kW/cm^2, which is well below the typical irradiance used during FCS (0.4~4 kW/cm^2) or SPT (0.1~0.25 kW/cm^2) experiments. SDS-PAGE electrophoresis (**Fig. 2-6**) shows that illumination in the presence of a sensitizer produces covalent Ras dimers at 42 kDa. On the other hand, Ras is strictly monomeric in the absence of either irradiation or fluorescent sensitizer bound to the protein, indicating that photochemistry, not other side effects such as heating, is responsible for the dimer formation. The degree of crosslinking is dependent on the type of dye as well as the illumination dosage. Dimers formed with all dyes tested, and trimers and tetramers are clearly visible in some cases. This is consistent with the SPT observations (**Fig. 2-4D**) indicating the presence of more than two species at high Ras density. The crosslinked Ras species generated by photosensitization were compared to the product of direct excitation of aromatic amino acid side chains by UV irradiation, and to that of enzymatic crosslinking by horseradish peroxidase (HRP) and

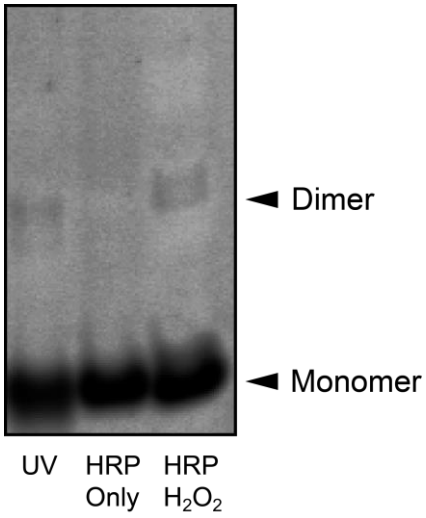

Figure 2-7. SDS-PAGE gel electrophoresis of Ras subjected to various oxidative stresses. H-Ras forms covalent dimers under the UV illumination and enzymatic oxidative stress.

hydrogen peroxide. Dimers are also formed by UV irradiation and HRP catalysis (**Fig. 2-7**), indicating that these well-known mechanisms involving reactive oxygen species (ROS) other than photosensitization can produce crosslinked products.

In order to gain insight to the location of the crosslinking site and the structural differences of dimers formed by different mechanisms, the fluorescence spectra of dityrosine in crosslinked Ras dimers were monitored. Dityrosine formation is one of the best characterized of oxidative crosslinking reactions, and is commonly studied in the context of protein degradation due to oxidative stress (96). Oxidation of tyrosine produces tyrosyl free radicals, which can react with each other to generate three isomers of dityrosine (97). The presence of dityrosine can be detected by fluorescence emission at 400 nm, which results from a shift in fluorescence wavelength of tyrosine at 300 nm upon the extended conjugation of the molecule (98). **Figure 2-8A** shows the fluorescence emission spectrum of the dityrosine generated from free L-tyrosine amino acids in HEPES buffer (pH 7.4) by irradiating a dye sensitizer (Alexa Fluor 488). The well-defined single band centered at 400 nm signifies the formation of dityrosine. The fluorescence spectra of dityrosine in crosslinked H-Ras, which contains nine tyrosine residues on the surface, by direct excitation of tyrosine (Type I photosensitization reaction) is similar to that of free dityrosine, and identical among the three H-Ras constructs (**Fig. 2-8B**). This suggests that dimers formed by direct radicalization of tyrosine are uniform in crosslinking sites and its overall structure.

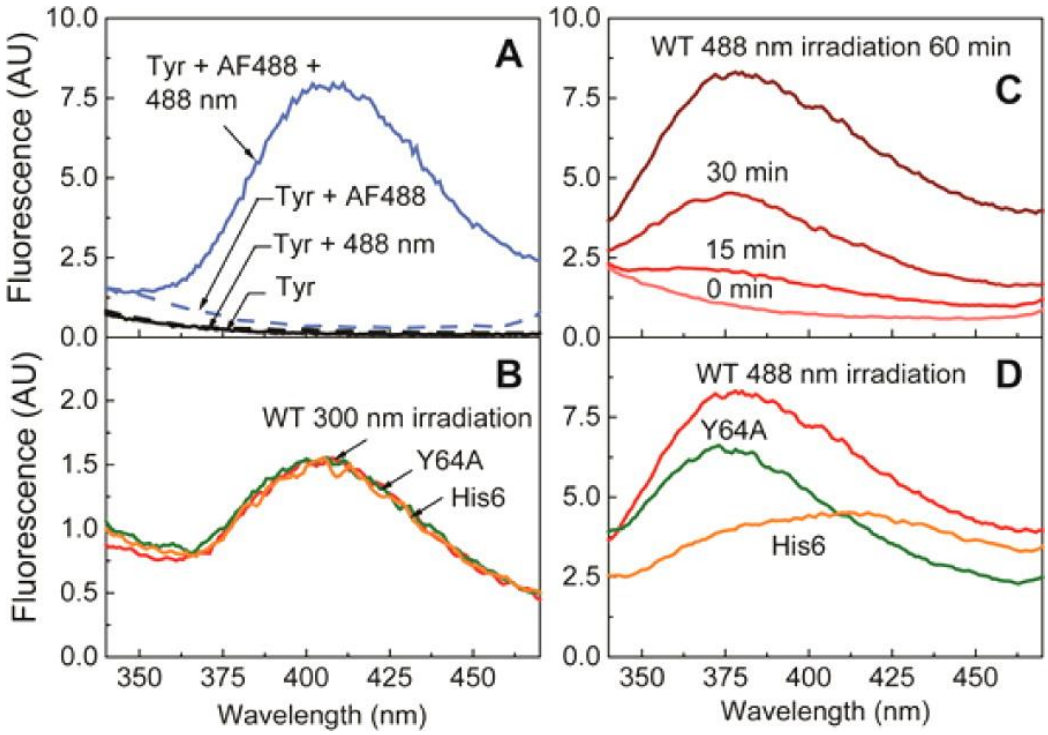

Figure 2-8. Dityrosine fluorescence emission spectra (λ_{ex} = 294 nm). (A) Free tyrosine in solution forms dityrosine in the presence of dye sensitizer (AF488) and laser illumination. (B) Crosslinked Ras products via UV illumination display a spectrum similar to that of free dityrosine. (C) Wild-type Ras in solution has an illumination dosage-dependent growth of the dityrosine band. (D) Three Ras constructs display different spectra, indicating that significantly different structures result from laser illumination.

Ras dimers formed by a Type II photosensitized reaction, where they are produced by fluorescent dye sensitization and laser irradiation, exhibit a fluorescence emission band slightly blueshifted from the free dityrosine band, and three different H-Ras constructs showed distinct spectral lineshapes. There is a significant broadening for the His6-tagged H-Ras, and even a single point mutation of Y64A results in an appreciably different spectrum from that of the wild type (**Fig. 2-8D**). This indicates that oxidative reactions can be sensitive to small differences in the amino acid sequence and produces significantly different structures. This is not surprising, as Type II photosensitization reactions are nonspecific in the sense that there is no single defined crosslinking site; rather, an ensemble of crosslinked dimers generated by different combinations of multiple possible crosslinking sites is expected. Furthermore, the position of the dye sensitizer relative to the protein may introduce additional structural sensitivity absent in Type I reactions, in which tyrosine is directly excited. These results indicate that crosslinking via tyrosyl free radicals is one of the reactions that contribute to covalent Ras dimer formation. Similar intermolecular dimerization reactions via dityrosine have been observed in other proteins such as calmodulin (99).

There are several factors that may cause membrane-bound Ras to behave differently from solvated Ras, such as effectively higher concentration, reduced orientational degrees of freedom, and interactions with the membrane. In light of the structural sensitivity of the Type II photosensitized Ras dimerization reaction reported above, one may assume that the membrane can introduce more structural identity and possibly

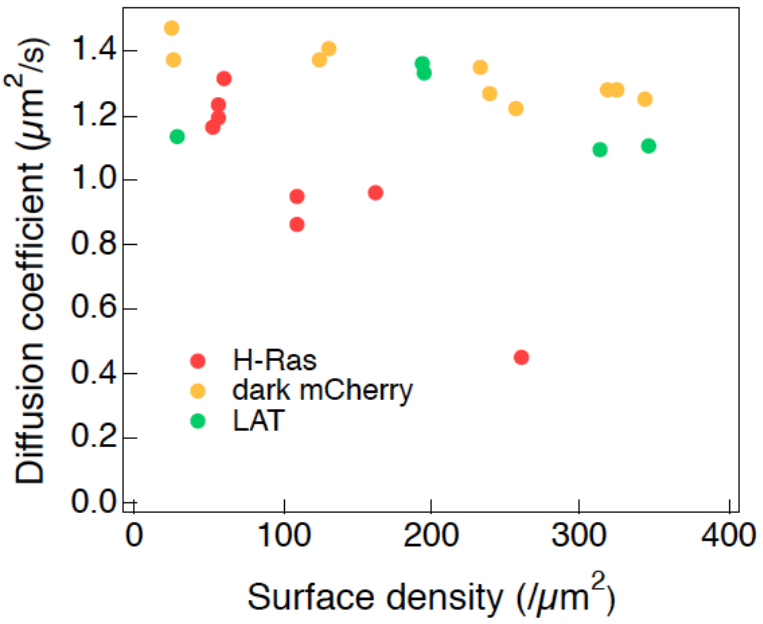

Figure 2-9. Density-dependent FCS for various proteins. Density-dependent diffusion coefficient of H-Ras-His6:ATTO488-GDP, dark mCherry-His10-Alexa Fluor 488, and LAT-His6-Alexa Fluor 555 measured by FCS. The dark mCherry has a Y67S point mutation, which renders the protein nonfluorescent (100). The proteins were coupled to the bilayer (4% Ni-NTA-DOGS, 96% DOPC) by Histidine tag-nickel chelation method (101).

enhance the differential susceptibility of Ras to these reactions. Indeed, such effects may underlie the observed differences between wild type Ras and the Y64A point mutant on membrane surfaces (84).

To provide context to the relative vulnerability of Ras to oxidative reactions, the degree of covalent crosslinking in other proteins in similar environments were evaluated. Density-dependent diffusion coefficient values were measured by FCS for H-Ras, the cytosolic domain of linker of activated T-cells (LAT), and nonfluorescent mCherry (mCherry S136C), all tethered to the membrane by polyhistidine tag chelated to Ni-NTA modified lipid (**Fig. 2-9**). LAT and nonfluorescent mCherry were labeled with the organic dyes Alexa Fluor 555 and 488, respectively. None of the proteins other than H-Ras showed significant density-dependent diffusion change, which suggests that Ras may be particularly sensitive to oxidative stress-driven dimerization. Its pronounced sensitivity to oxidative crosslinking may be attributed to the unusually high density of reactive amino acid residues on the surface: H-Ras has nine Tyr, four His, and one Cys residues exposed on the surface, which is significantly higher in density compared to LAT or mCherry. Incidentally, other small GTPases of similar sizes such as Rac1, RhoA, Rab1A, and Rap1A also have substantially lower numbers of exposed Tyr, His, Trp, and Cys per unit surface area (**Table 2-1**). In addition to the number of surface-exposed reactive amino acids, their relative orientation with respect to each other may play a role in determining a protein's sensitivity to oxidative crosslinking.

Table 2-1. Comparison of the number of oxidation-sensitive amino acid residues exposed on the surface for various GTPases and mCherry. Crystal structure was analyzed using UCSF Chimera. Chimera is developed by the Resource for Biocomputing, Visualization, and Informatics at the University of California, San Francisco (102).

	PDB ID	Tyr	His	Trp	Cys	Surface area (Å^2)
H-Ras	4EFL	9	4	0	1	7662
Rac1	3TH5	4	2	1	2	7413
RhoA	1FTN	3	2	1	0	8106
Rab1A	2FOL	7	1	2	1	7160
Rap1A	3ZFI	0	4	0	0	8073
mCherry	2H5Q	4	5	0	0	9226

Discussion

We have shown intermolecular crosslinking of H-Ras on membranes through a mechanism most consistent with a Type II photosensitized reaction. Reactive singlet oxygen species, catalytically generated by repeated excitation and quenching of a photosensitizer dye, create free radicals and ultimately protein cross linking via susceptible amino acids such as tyrosine. These photosensitized oxidative reactions have been known since the beginning of biological fluorescence experiments (103-105). The crosslinking reactions, though inherently nonspecific, are remarkably sensitive and even a point mutation can significantly alter the product distribution. This last point should be taken with a cautionary note, since comparative studies between point mutations are often regarded as the most definitive demonstrations of specificity in experimental results. In regard to the question of Ras dimerization on membranes, these findings may explain discrepancies in recent literature (66, 67, 82-84, 106). More importantly, the distinct predisposition of Ras to such reactions raises the possibility that Ras experiences similar reactions in the cellular context, where reactive oxygen species are abundant and even participate in the signaling network at various points (107).

Materials

Fluorescent nucleotides ATTO488-GDP, ATTO488-GppNHp, ATTO594-GTP, and ATTO647N-GTP (Cat# NU-840-488, NU-860-488, NU-820-594, NU-820-647N) were purchased from Jena Biosciences (Jena, Germany). Lipids (1,2-di-(9Z-octadecenoyl)-sn-glycero-3- phosphocholine, DOPC; 1,2-dioleoyl-sn-glycero-3-phospho-L-serine, DOPS; 1,2-dioleoyl-sn-glycero-3-phosphoetahnolamine-N-[4-(p-maleimidomethyl)cyclohexane-carboxamide], MCC- DOPE) were purchased from Avanti Polar Lipids. Texas-Red DHPE (Cat# T-1395MP) was purchased from Life Technologies (now ThermoFisher Scientific, South San Francisco, CA). Ethylenediaminetetraacetic acid (EDTA), L-tyrosine, guanosine triphosphate (GDP), 5'-guanylyl imidodiphosphate (GppNHp), and other buffer components were purchased from Sigma-Aldrich (St. Louis, MO). Imaging buffer consisted of β-mercaptoethanol (BME), glucose, Trolox, glucose oxidase, and catalase. All components were purchased from Sigma-Aldrich except glucose oxidase, which was purchased from Serva Electrophoresis GmbH (Heidelberg, Germany).

Methods

H-Ras purification

A modified H-Ras with the following sequence was purified in the E. coli bacterial purification system reported in detail elsewhere (40):

MTEYKLVVVG	AGGVGKSALT	IQLIQNHFVD	EYDPTIEDSY
RKQVVIDGET	CLLDILDTAG	QEE**<u>Y</u>**SAMRDQ	YMRTGEGFLC
VFAINNTKSF	EDIHQYREQI	KRVKDSDDVP	MVLVGNKSDL
AARTVESRQA	QDLARSYGIP	YIETSAKTRQ C	GVEDAFYTLV
REIRQHKLRK	LNPPDESGPG		

The terminal cysteine serves as the reaction site to bind the protein to the bilayer. The underlined Y denotes the location of the Y64A mutation. His6 construct contained six histidine residues at the C-terminus.

Sample preparations for Ras on supported lipid bilayers

Membrane-bound H-Ras samples were prepared for FCS and SPT experiments. Relevant protocols have been reported in detail previously (59). Briefly, supported lipid bilayer was formed by rupture of small unilamellar vesicles (SUVs), prepared by extrusion, on glass substrates cleaned by piranha etch. A typical batch of SUVs were prepared in the following lipid composition: 2% MCC-DOPE, 2% DOPS, 96% DOPC and a trace amount (0.0025 – 0.01%) of Texas Red-DHPE. The bilayers were prepared in ibidi sticky-Slide VI 0.4 chambers (ibidi GmbH, Martinsried, Germany) for imaging. H-Ras was tethered to the bilayer via thiol-maleimide conjugation between the terminal cysteine (C181) and maleimide in the headgroup of MCC-DOPE lipids. Native nucleotide cofactors were exchanged for ATTO488-labeled guanosine nucleotides after being stripped with 50 mM EDTA. The final sample was in 50 mM HEPES, 150 mM NaCl, and 5 mM $MgCl_2$. The imaging buffer was of the following composition: 10 mM BME, 20 mM glucose, 2 mM UV-treated Trolox, 320 μg/mL glucose oxidase, and 50 μg/mL catalase in the HEPES buffer (92, 108, 109).

Ras crosslinking reactions in solution

Laser irradiation

Cys181 residue in H-Ras was capped with 10-fold molar excess maleimide for 30 min at room temperature to avoid potential disulfide crosslinking. Endogenous nucleotides in Ras were exchanged with desired fluorescent or dark GDP before light illumination. In a typical exchange reaction, Ras was incubated with 25 mM EDTA in 50 mM HEPES/150 mM NaCl buffer for at 4 °C for 30 min to chelate Mg^{2+} which is a cofactor for guanine nucleotide binding. EDTA and released endogenous nucleotide were removed by buffer exchange with 50 mM HEPES/150 mM NaCl using size exclusion spin column (Bio-Rad). A two-fold molar excess of desired nucleotides with respect to Ras was incubated overnight at 4 °C in the presence of 5 mM of Mg^{2+}. Ras concentration was adjusted to be 1 mg/ml for light illumination experiments. For free tyrosine experiments, 0.1 mM L-tyrosine (Sigma-Aldrich) and 10 μM Alexa Fluor 488 (Life Technologies) in HEPES buffer was illuminated using identical conditions.

UV irradiation

H-Ras labeled with dark GDP were illuminated with 306-nm-UV light for 60 min. To avoid heating the solution, illumination was paused every 10 min and the solution was cooled down in an ice bath for 10 min.

HRP-peroxide crosslinking

Enzymatic oxidative reactions were catalyzed by horseradish peroxidase (HRP) in the presence of hydrogen peroxide as the oxidizing agent. HRP has a similar molecular weight to H-Ras dimer, and thus appears overlapped with H-Ras dimer in the SDS- PAGE gel. This could be an issue to detect H-Ras dimer. In order to circumvent this issue, we used HRP-magnetic microparticle complexes, and completely removed HRP after enzymatic re-actions using magnetic separator (Invitrogen). 10 μL of HRP stock solution (Invitrogen) was incubated with 0.5 mg of magnetic particles (Promega) for 30 min to physically adsorbed HRP on the particle surfaces. Unbound HRP was removed by washing three times with PBS followed by an additional washing with 50 mM HEPES/100 mM NaCl/5 mM $MgCl_2$. 50 μL of 1 mg/mL H- Ras was reacted with 0.1 mg of HRP-magnetic particle complexes in the presence of 10 mM of H_2O_2 for 30 min. After reaction, supernatant containing H-Ras was collected after HRP-magnetic particle complexes were removed by magnetic separation. The supernatant was centrifuged at 1500 g for 5 min to remove residual particles. The top layer was carefully collected and loaded into gel electrophoresis.

SDS-PAGE Gel Electrophoresis

The precast polyacrylamide gels used in the study were NuPAGE Novex 4-12% Bis-Tris protein gels (Life Technologies). Running buffer was prepared from 1 M Tris base, 1 M 2-(N- morpholino)ethanesulfonic acid (MES), 20.5 mM EDTA and 2% sodium dodecyl sulfate (SDS). Ras proteins diluted to 1 mg/mL, as confirmed using NanoDrop 2000 (Thermo Scientific), were mixed with lithium dodecyl sulfate sample buffer (Life Technologies) and MilliQ water at a ratio of 2:1:1. The samples were heated at 95^{o}C for 3 min on a heat block before they were loaded into individual wells. The electrophoresis

process was set at 200 V, 400 mA. The gels were subsequently transferred to a plastic container with DI water, and stained with Sypro Ruby protein gel stain (Molecular Probes) using the rapid staining protocol. The gels were imaged using a benchtop 2UV transilluminator at 302 nm.

Fluorescence Correlation Spectroscopy

Dual-color FCS was performed on a home-built setup with a modified inverted microscope (Nikon TE2000). For excitation, wavelengths selected by bandpass filters from a pulsed white light laser source (SuperK Extreme EXW-12, NKT Photonics, Copenhagen, Denmark) were used. The excitation pulses are sent into a single mode optical fiber, then the combined pulses enter the microscope via a multi-color dichroic cube (Di01-R405/488/561/635-25x36, Semrock). Notch filters were used to remove excess excitation intensity. The fluorescence signal is collected by the 100x high-NA oil immersion objective, and recorded by avalanche photodiode detectors (Hamamatsu). The signal is directly converted into autocorrelation signal by a hardware correlator (Correlator.com). In the experiments described in the text, blue light (488 nm) was used to excite the ATTO 488 fluorophore, and orange light (568 nm) for exciting Texas Red-DHPE simultaneously. The average power used to excite the sample ranged between 0.5 and 5.0 μW de- pending on the fluorophore quantum yield and the surface density, which is equivalent to the irradiance range of $0.4 \sim 4.0$ kW/cm^2 calculated with the calibrated spot sizes. The resulting auto-correlation $G(\tau)$ was fit to the two-dimensional Gaussian diffusion model:

$$G(\tau) = \frac{1}{N}\left(\frac{1}{1+\tau/\tau_D}\right) \quad \textbf{[2-1]}$$

Where τ is time delay, N is the number of particles in the focus spot, τ_D is the correlation time. To calibrate the spot size of the confocal focus, N of a bilayer with a known surface density of fluorescent lipids of each color, BODIPY-FL-DHPE (Life Technologies) for 488 nm and Texas Red-DHPE for 568 nm, were measured, which consistently yielded the radius of 0.20 ± 0.01 μm and 0.22 ± 0.01 μm for 488 nm and 568 nm, respectively. The diffusion coefficient D was calculated by using the relation:

$$D = \frac{w^2}{4\tau_D} \quad \textbf{[2-2]}$$

Where w is the radius of the focus spot size.

Single Particle Tracking

Single-molecule imaging experiments were performed on a Nikon eclipse Ti inverted micro-scope with a 100× 1.49 N.A. oil immersion TIRF objective and iXon EMCCD camera (Andor Technology Ltd., UK). 640 nm (RCL-050-640, Crystalaser, NV), 561 nm (Sapphire HP, Coherent Inc., CA) and 488 nm (Sapphire SF, Coherent Inc., CA) were used as illumination sources for TIRF imaging. A dark background before single-molecule imaging was achieved typically by a 20-s photobleaching with the laser power of 20 mW at the objective. Single-molecule data were quantified using an ImageJ plugin (TrackMate) (110) and analyzed in Igor Pro (WaveMetrics).

The step size distribution for each sample was fit with both the single- and two-component Brownian diffusion model. The probability density for a particle with diffusion coefficient (D) to move a distance (r) in time interval (t) is:

$$p(r,t,D) = \frac{r}{2Dt}\exp\left(-\frac{r^2}{4Dt}\right) \quad \textbf{[2-3]}$$

Therefore, two-component diffusion with two different diffusion coefficients (D_1 and D_2) and the relative population for the first component (α) is described by the following equation:

$$p(r,t,D) = \frac{\alpha r}{2D_1 t}\exp\left(-\frac{r^2}{4D_1 t}\right) + \frac{(1-\alpha)r}{2D_2 t}\exp\left(-\frac{r^2}{4D_2 t}\right) \quad \textbf{[2-4]}$$

Fitting residues for the single- and two-component model were monitored to determine the number of diffusion species. The diffusion coefficients and relative population of each component were calculated from the corresponding fitting.

3. Primary mode of SOS catalysis is through processive Ras activation by single proteins[2]

Introduction

Son of Sevenless (SOS) acts as a central regulator of signal transduction by controlling Ras activation (28, 29, 53, 111, 112). The ubiquitously expressed guanine nucleotide exchange factor (GEF) is cytosolic prior to membrane recruitment mediated by the adaptor Grb2 in response receptor tyrosine kinase (RTK) activation (32, 113-116). Membrane-bound, catalytically-activate SOS primes activation of the small GTPase, Ras. Once activated, Ras interacts with a multitude of downstream effector proteins, which results in a variety cellular outcomes including proliferation, differentiation, and survival (23). SOS is autoinhibited and its deregulation amplifies Ras signaling. For example, N- and C-terminal domain mutations in SOS have been shown to cause Noonan Syndrome and hereditary gingival fibromatosis due to augmented Ras signaling and subsequent increase in ERK activation (117-120). Thus, it is essential that SOS activation is tightly regulated under physiological conditions.

The complex domain architecture of SOS works collectively to autoregulate its activity (**Fig. 3-1A**) (34-37). The catalytic core of SOS, denoted SOS^{cat}, contains two Ras binding sites: the

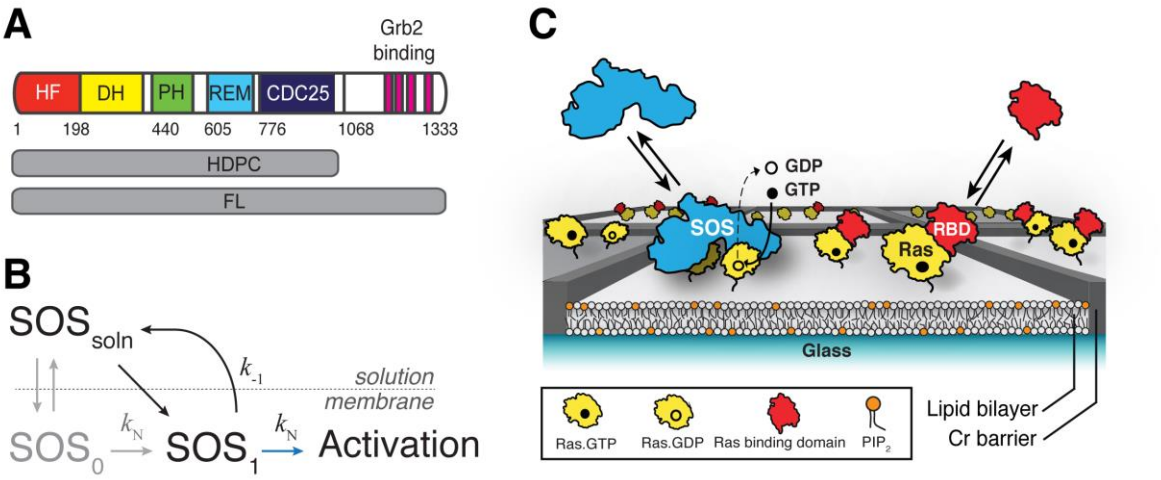

Figure 3-1. Single molecule SOS-catalyzed Ras activation assay on supported membranes. (A) Domain architecture of SOS constructs studied using the Ras activation assay. HF: histone-fold, DH: Dbl homology, PH: pleckstrin homology, REM: Ras exchanger motif. SOS lacking the Grb2 binding domain ($SOS^{hdpc)}$ and the full-length ($SOS^{FL)}$ enzyme are depicted in gray bars. (B) Chemical kinetic model of SOS activation including recruitment from the cytoplasm and full activation at the membrane. Receptor-independent SOS activation (black) lacks membrane recruitment and dissociation steps mediated by activated receptors (gray). (C) Schematic of Ras activation by SOS on the supported membrane microarray. Ras activation is measured using a sensor derived from the Ras binding domain (RBD) of CRaf.

[2] This chapter is from the manuscript in preparation co-first authored by H. Y. M. Lam and S. Alvarez. Special acknowledgements to S. T. Low-Nam for the helpful discussion and advice on the manuscript.

catalytic pocket at the cdc25 domain, and the allosteric pocket located between the REM and cdc25 domains. SOS^{cat} has a built-in positive feedback loop wherein allosteric site binding to its own product leads to Ras activation enhancement via two mechanisms (53, 121). Allosteric-Ras.GTP engagement increases nucleotide exchange rate of Ras at the catalytic site (38, 69) and frequency of SOS recruitment to the membrane increases due to the increased affinity of Ras.GTP at the allosteric pocket (36, 70). This regulation allows SOS to integrate analogue inputs to generate digital signaling in lymphocytes (121-124). On the other hand, domains flanking SOS^{cat}, which constitute the regulatory subunit, autoinhibit SOS activity until all required inputs are present. The histone fold (HF), Dbl-homology (DH), and Pleckstrin-homology (PH) domains at the N-terminus cooperatively block allosteric Ras binding (36, 72), which is released through interactions with negatively charged lipids (40, 72, 125). The C-terminal proline-rich (PR) domain provides complementary, yet independent obstruction of the allosteric pocket (71). The mechanism by which PR-domain autoinhibition is relieved is incompletely understood but both membrane recruitment and interaction with Grb2 are considered to be essential (37, 70, 71). Together, the two terminal subunits of SOS enable efficient Ras activation while preventing spurious signaling.

A single SOS molecule can processively turnover thousands of Ras over the course of minutes (39, 70, 71). This hyperactive state was discovered due to the key innovation of measuring single molecule SOS catalysis on Ras-functionalized supported membrane systems. The processive state can be accessed once SOS is allosterically activated and stably anchors to the membrane via Ras engagement at both catalytic and allosteric pockets (39, 70). Although the mean catalytic rate of hyperactive SOS^{cat} molecules is insensitive to the nucleotide state of Ras, Ras.GTP mediates SOS fluctuations into higher activity states (39). Single molecule measurements of SOS (1-1049) with a truncated PR domain (SOS^{hdpc}) and endogenous full-length protein (SOS^{FL}) from cell lysate show that N- and C-terminal domains significantly reduce SOS membrane-recruitment (70, 71). However, the processive behavior observed in SOS^{cat} is unaffected by the flanking regulatory domains. Further, upon receptor stimulation in B cells, SOS molecules that are recruited to the plasma membrane remain bound until they are actively removed through endocytosis (70). These studies have established the potency of Ras activation achieved by activated single SOS molecules.

While SOS molecules stably associated to membrane demonstrate processivity in Ras turnover, it remains unknown whether SOS that is initially autoinhibited can access such a state. This has been due, in particular, to challenges in purification of SOS^{FL} for *in vitro* studies. The C-terminal domain strengthens obstruction to the allosteric pocket, but it is unclear if this mechanism completely abolishes SOS activation of Ras in the absence of receptor-mediated recruitment (71). Furthermore, the effects of catalyzed Ras deactivation, for example by GTPase activating proteins (GAPs), on the ability for single SOS to robustly activate Ras remain elusive. No platform currently exists to quantitatively measure the catalytic effects of GEFs and GAPs on Ras while resolving the activity of single enzymes.

We extend the single molecule SOS activation assay by characterizing Ras activation kinetics of purified SOS^{hdpc} and SOS^{FL} on supported lipid bilayers (SLBs). These assays are initiated with inactive, GDP-bound Ras. The absence of Ras.GTP mimics the condition of non-stimulated cells, thus bypassing the receptor-mediated pathway of SOS activation (**Fig. 3-1B**). Additionally, we developed a fluorescently labeled Ras binding domain (RBD) of CRaf to measure real-time Ras activation. This sensor enables quantitative measurements of SOS activity for more than an hour with no loss in sensitivity as well as the ability to detect GAP-catalyzed deactivation of Ras. Measurements reveal that, although rare, inactive SOS^{FL} can transition into the hyperactive state and processively activate thousands of Ras molecules. A transiently active state of SOS with low catalytic activity was observed in addition to the processive state. However, adding low concentrations of the GAP-domain of NF1 (NF1-333) eliminated the ability for SOS in the transient state to activate Ras. On the other hand, processive SOS molecules were still capable of causing bursts in Ras activation in the presence of GAP activity, indicating that Ras is primarily activated by single molecules of SOS in the processive state. Furthermore, allosteric activation of SOS by Ras.GTP is primarily manifested as an enhanced probability for SOS to fluctuate into the processive activity state. Our findings indicate that other mechanisms, such as tight spatiotemporal control of Ras clusters, must be in place to prevent spurious Ras activation by processive SOS.

Results

Real-time Ras activation assay

Single molecule SOS processivity has been established using SOS that is captured on the membrane in the absence of free nucleotides on H-Ras-functionalized supported membranes (39, 70, 71). We introduce the real-time Ras activation assay that extends earlier measurements to quantify SOS catalytic activity without the requirement for SOS to be stably associated with the membrane *ab initio*. A supported lipid bilayer (SLB) was segmented into micrometer-sized regions using nanofabricated chromium barriers such that membrane-recruited SOS molecules would be constrained into separate regions for single-protein activity characterization (**Fig. 3-1C**). H-Ras (1-181, C118S), hereafter termed Ras, molecules were permanently tethered to maleimide-functionalized lipids via the C-terminal cysteine (see Methods for details). All Ras molecules were loaded with GDP prior to the addition of SOS.

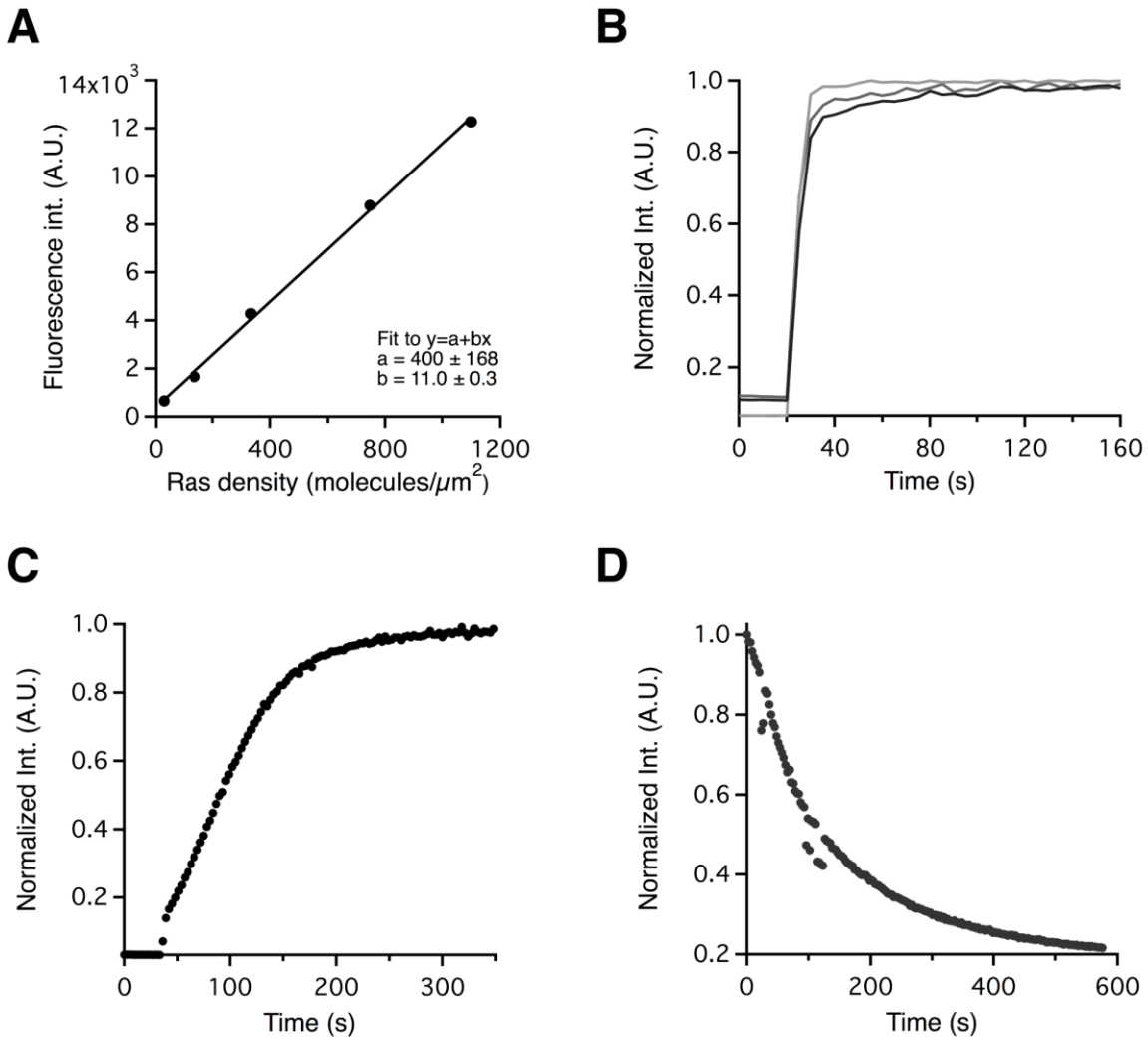

Figure 3-2. Characterization of fluorescent RBD sensor. (A) Calibration curve to convert fluorescently labeled RBD sensor to Ras.GTP density. (B) Equilibration time of fluorescent RBD sensor on Ras.GppNp-decorated SLBs (n=3). (C,D) Fluorescent RBD sensor is sensitive to Ras activation by 5 nM SOS^{cat} labeled with Alexa 647 (C) and Ras deactivation by 1 nM NF1-333 (D) in bulk measurements.

We added a new dimension to the assay by developing a Ras activation sensor that enables quantitative measurement of Ras.GTP levels with second time resolution and is stable for up to hours. The sensor is a SNAP-tagged Ras binding domain (RBD) of CRaf with a K65E point mutation and labeled with a benzylguanine Alexa-488 dye. Since the RBD sensor is labeled, the use the fluorescent nucleotides is no longer required, which permits the use of native nucleotides and allows Ras.GTP level to be measured with high sensitivity over longer timescales compared to the fluorescent nucleotide exchange assay. The mutation was introduced due to the five-fold increase in dissociation constant compared to the wild-type construct (126), which minimizes competition between SOS and RBD sensor binding to Ras. RBD sensor intensity was linearly correlated with Ras.GTP densities up to 1,200 molecules/μm^2 (**Fig. 3-2A**). The sensor rapidly equilibrates between the solution and Ras.GTP on the membrane (**Fig. 3-2B**). The fast equilibration kinetics enable detection of Ras activation from a single, processive SOS molecule, which can turn over thousands of Ras-bound nucleotides within minutes (39, 70, 71). Furthermore, the RBD sensor enables measurement of both Ras activation and deactivation catalyzed by GEFs and GAPs, respectively. This is further demonstrated by the response of the sensor to catalytic activity of SOS^{cat} and the GAP domain of NF1, termed NF1-333, on Ras on SLBs (**Fig. 3-2C, D**).

In a typical experiment, the RBD sensor, SOS, and GTP were simultaneously added to Ras-decorated SLBs via microinjection and maintained in solution at constant concentration throughout the experiment. All activity states of SOS were measured based on RBD sensor recruitment using total internal reflection fluorescence microscopy (TIRFM). The fast on rate for sensor binding enabled measurement of SOS states with low activity in which SOS was not first stably recruited to the membrane (**Fig. 3-3A, B**). At the end of each experiment, high concentrations of SOS^{cat} and GTP were added to fully activate all Ras molecules to measure total Ras density in each corral (see Methods). Corrals within a field of view have similar Ras densities with small variation.

SOS^{hdpc} exhibits two distinct Ras activation modes

Two types of reaction trajectories characterized Ras activation catalyzed by SOS^{hdpc}: one with relatively linear activation throughout image acquisition (**Fig. 3-3B** pink line), and another that exhibited sudden bursts in Ras activation (**Fig. 3-3B** blue line). The linear activation mode resulted in a two-fold increase in Ras.GTP after 30 minutes compared to the intrinsic nucleotide exchange measured in the absence of GEFs (**Fig. 3-3B** black line). Thus, this mode of activation is capable of contributing a measurable, yet minor amount of catalysis to Ras activation. On the other hand, the second activity mode showed much more potent Ras activation. Thousands of Ras were activated over minutes and the onset of activation bursts corresponded to the detection of single SOS molecules (**Fig. 3-4A**). The activation rate distribution of identified bursts matches the nucleotide turnover rates measured by individual membrane-bound SOS in fluorescent nucleotide exchange assays (**Fig. 3-4B**, see Methods) (39, 70, 71), indicating that stably recruited single SOS molecules are, indeed, the cause of bursts in Ras activation.

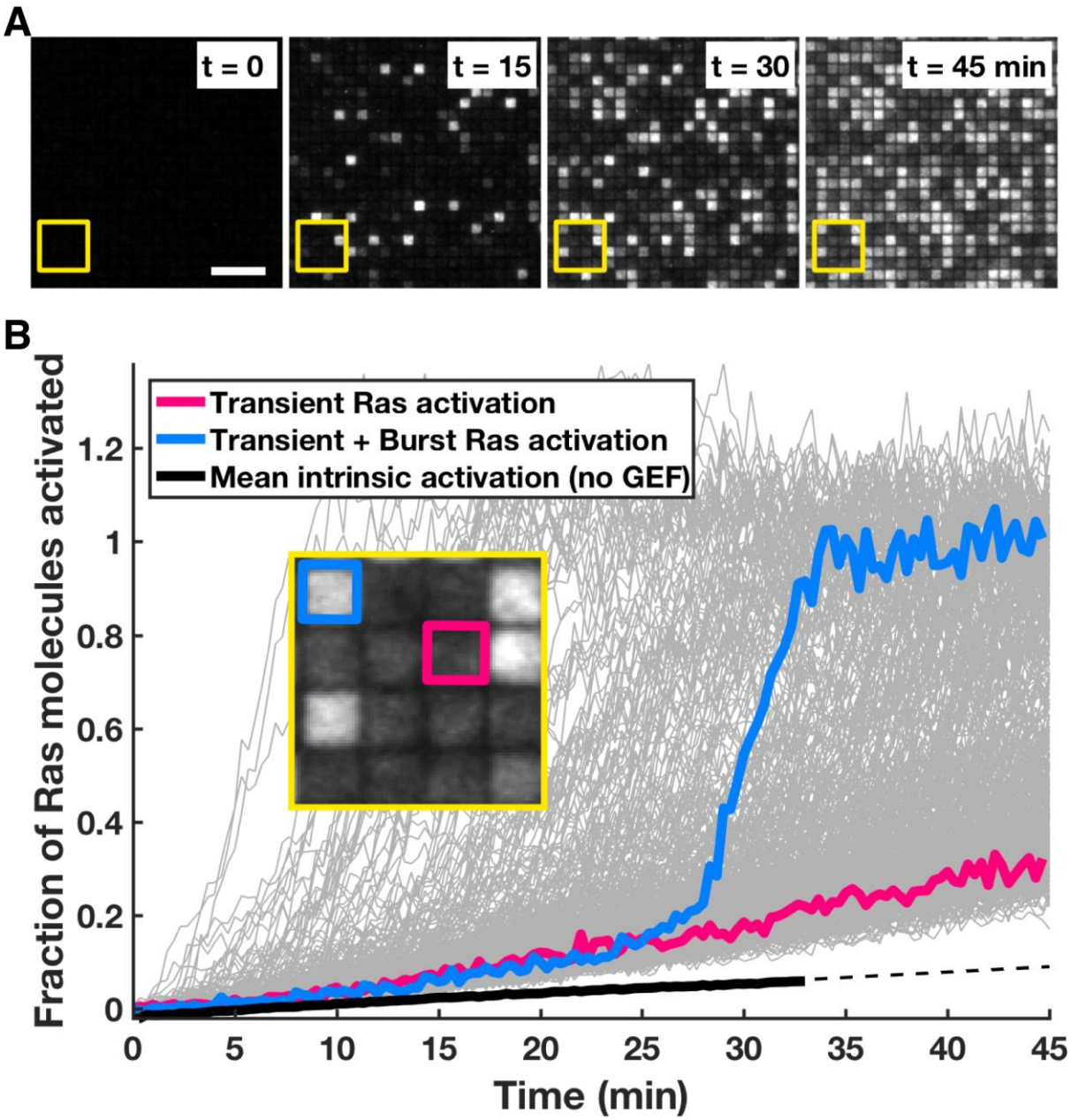

Figure 3-3. SOS^{hdpc} exhibits transient and processive Ras activation. (A) TIRFM images of fluorescent RBD sensor used to quantify Ras.GTP levels in each corral (n=576) at 0, 15, 30, and 45 minutes after addition of 10 nM SOS^{hdpc} to Ras.GDP-tethered SLB. Number of Ras per corral is 4000 ± 250 molecules. Scale bar = 10 μm. (B) Ras activation traces of all corrals shown in (A). Two representative corrals and traces show reactions in which transient Ras activation (pink) and both transient and burst Ras activation (blue) occur. All other reaction trajectories are shown in gray. Mean Ras activation trace via intrinsic nucleotide exchange (n=600) is shown in black.

Corrals that experienced linear activation were primarily activated by SOS with transient membrane interactions. In three representative time-lapses where SOS was imaged with 20 millisecond time resolution, only two identifiable SOS molecules, which dwelled on the membrane for less than 10 s, were detected over a total of 84 minutes before bursts in Ras

activation were observed. This result suggests that slow Ras activation was caused by SOS which interacted with the membrane for less than 20 ms and, thus, had limited potential for Ras binding and activation. SOS which were temporarily recruited to the membrane are henceforth termed as being in the transient state, whereas stably recruited SOS that rapidly activated Ras are in the processive state.

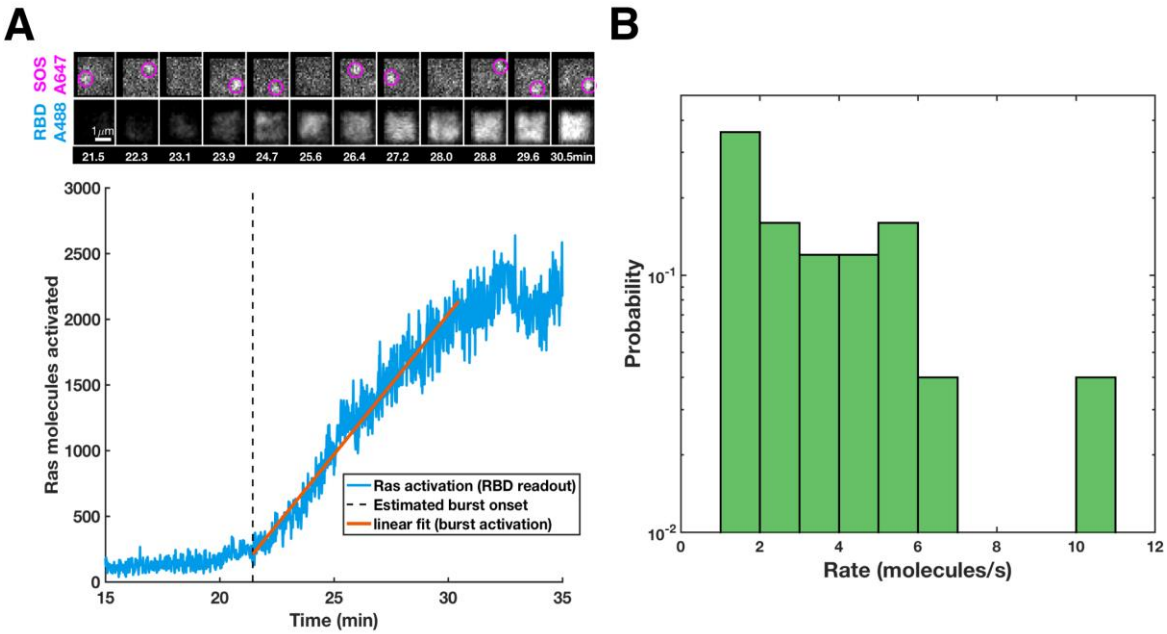

Figure 3-4. Bursts in Ras activation are catalyzed by stably-recruited single SOS molecules. (A) TIRFM images of Alexa 647-labeled SOS^{hdpc} (top row) and fluorescent RBD sensor (bottom row) tracked in a single corral over 9 minutes starting at the onset of rapid Ras activation (dashed line). Identified single molecules of SOS are circled in pink, and frames with no observable SOS are due to fluorophore blinking (127). The number of Ras molecules activated in the corral between 15 and 35 minutes after SOS addition is plotted in blue, and linear fit used to calculate rate of Ras activation is shown in orange. Scale bar = 1 μm. (B) Histogram of burst Ras activation rates catalyzed by 10 nM SOS^{hdpc}.

Allosteric enhancement of SOS^{hdpc} activity by Ras.GTP

We confirmed allosteric activation of SOS^{hdpc} in the form of enhanced catalytic activity by Ras.GTP. The effect of Ras.GTP on SOS^{hdpc} activity was assessed by comparing Ras activation rates with and without Ras.GTP priming (see Methods). SOS^{hdpc} was added to membranes with comparable Ras.GDP densities with one including additional Ras.GTP at ~1:1 ratio with Ras.GDP (**Fig. 3-5A**, **Fig. 3-6A**). The Ras.GTP level in each corral was measured with the RBD sensor and the effective catalytic rate constant (k_{eff}) was calculated from transient state traces over the course of the first 10 minutes of the reaction (**Fig. 3-6A**, Methods). When Ras.GDP and Ras.GTP were both present on the membrane at the time of SOS addition, SOS^{hdpc} activated Ras at a mean k_{eff} of 6 x 10^4 s^{-1} M^{-1}, which is ten-fold greater than the condition without initial Ras.GTP (**Fig. 3-5A**). Thus, SOS^{hdpc} catalysis is sensitive to the Ras-bound nucleotide state. Since the rate of SOS-mediated Ras turnover is independent of the nucleotide state at the catalytic pocket (53), SOS in the transient state requires Ras engagement at both allosteric and catalytic sites, in support of previous structural studies (38, 69, 128).

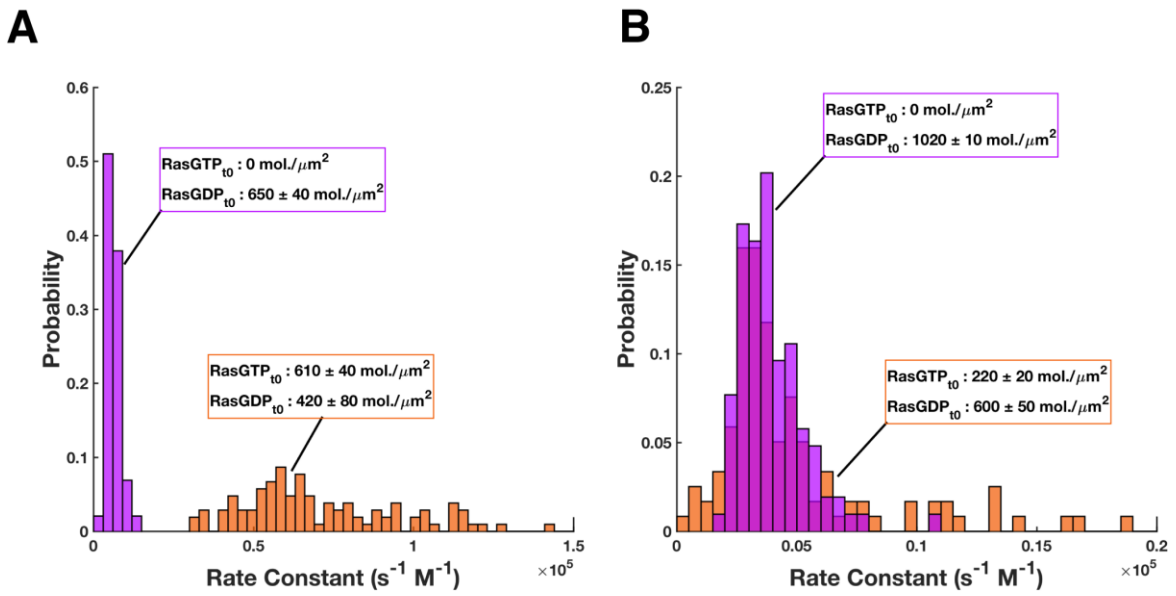

Figure 3-5. SOS C-terminal domain inhibits allosteric activation by Ras.GTP in the transient activation mode. (A,B) Distributions of effective catalytic rate constant (k_{eff}) of SOS^{hdpc} (A) and SOS^{FL} (B) in the transient activation state on Ras.GDP SLBs with and without addition of Ras.GTP. k_{eff} distributions are shown in the absence of Ras.GTP (magenta) and with a fraction of initial Ras.GTP prior to SOS exposure (orange). The mean Ras.GDP and Ras.GTP densities in corrals before measurement are displayed for each distribution.

SOS C-terminal domain suppresses allosteric activation

The mechanism of SOS^{FL} allosteric activation by Ras.GTP remains elusive due to the challenges of purifying the full-length protein. The difficulty of obtaining SOS^{FL} was recently overcome by capturing SOS^{FL} from whole cell lysates, which were studied using the single molecule SOS activity assay (71). Our study presents one of the first direct measurements of catalytic activity of SOS^{FL} expressed and purified in bacteria.

Unlike SOS^{hdpc}, SOS^{FL} in the transient activation state did not exhibit allosteric activation by Ras.GTP. The distribution of SOS^{FL} k_{eff} values were similar with an identical mean k_{eff} of 0.3 x 10^4 s^{-1} M^{-1} in the absence or presence of Ras.GTP priming (**Fig. 3-5B**). The mean rate of Ras activation by SOS^{FL} was almost identical to that of intrinsic nucleotide exchange even with available Ras.GTP (**Fig. 3-6B**, **Fig. 3-3B** black line). The insensitivity of SOS^{FL} catalytic activity to Ras-bound nucleotide state indicates that the PR domain adds an additional layer of autoregulation through inhibition of Ras binding at the allosteric site, the catalytic site, or both pockets. Therefore, SOS^{FL}, in contrast to its truncated versions, rarely achieves the transient activation state.

Ras.GTP modulates SOS probability to enter processive state

Previous studies have shown that positive feedback in SOS is manifested as increased catalytic activity (38, 69) or increased membrane-recruitment (36, 70) upon allosteric-Ras.GTP binding. The observation that Ras.GTP had no effect on SOS^{FL} catalytic activity suggests that active Ras provides positive feedback to SOS via augmented recruitment to the membrane. Since rapid Ras.GTP production was detected in samples with added SOS^{FL}

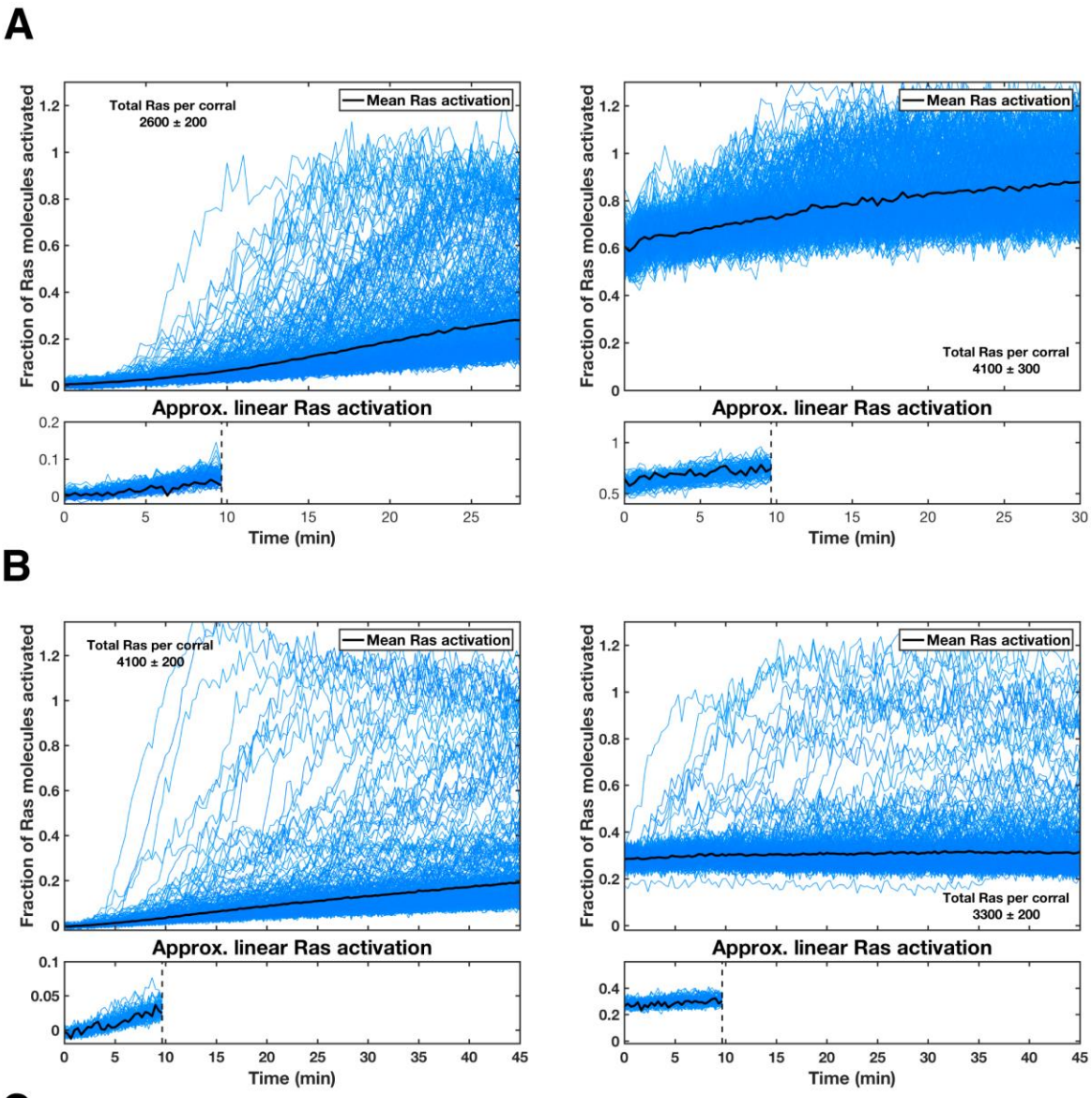

Figure 3-6. Analysis of Ras.GTP effects on Ras activation catalyzed by SOS^{hdpc} and SOS^{FL} in the transient activation mode. (A,B) Traces of Ras activation traces catalyzed by SOS^{hdpc} (A) and SOS^{FL} (B) on inactive Ras bilayers (left plots) and on bilayers with a mixture of active and inactive Ras (right plots) at the beginning of measurement. All traces (n=600 per plot) are in blue and the mean trace is in black. Traces with no detected bursts in Ras activation in the first 10 minutes (narrow plots) were linearly fitted to determine initial rates and calculate the effective catalytic rate constant (k_{eff}). (C) Histogram of number of Ras.GTP molecules in each corral 10 minutes after SOS^{hdpc} addition in one sample. The distribution is fitted to a Gaussian curve and corrals that fall below the mean plus 2 times the standard deviation were selected to calculate k_{eff} values. This process was repeated for SOS^{FL}.

Fig. 3-6B), we investigated if Ras.GTP modulated the probability of SOS^{FL} to transition from the autoinhibited state to the processive state.

The number of burst Ras activation events catalyzed by SOS^{hdpc} or SOS^{FL} relative to Ras.GTP level was measured on SLBs starting with Ras.GDP. Traces with bursts in Ras activation were selected and the onset of each burst was identified using a change-point algorithm (see Methods, **Fig. 3-7A**). The number of burst activation events was determined as a function of the number of Ras.GTP molecules on the membrane (**Fig. 3-8B, C** left).

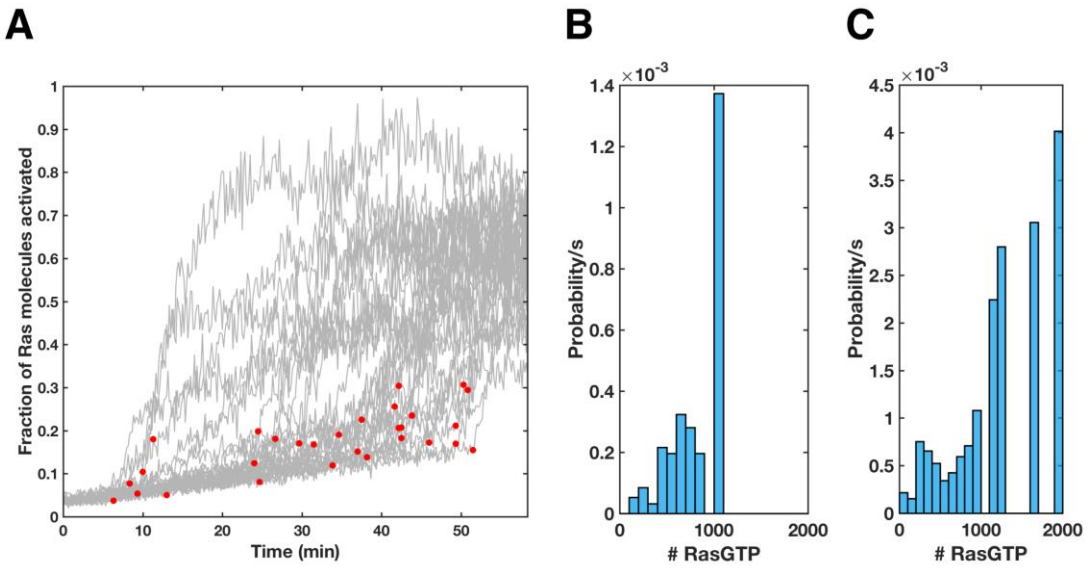

Figure 3-7. Probability of SOS entering the processive activation state is enhanced by Ras.GTP. (A) Ras activation traces with detected bursts in Ras.GTP production by SOS^{hdpc} (gray). The starting point of each burst activation event is indicated (red dots). (B,C) Normalized probability of SOS entering the processive state as a function of number of Ras.GTP for SOS^{hdpc} (B) and SOS^{FL} (C).

To quantify the effects of Ras.GTP, the amount of time SOS is exposed to Ras.GTP must be accounted for. SOS was primarily exposed to low levels of Ras.GTP (<600 Ras.GTP molecules in each corralled region) throughout image acquisition (**Fig. 3-6A, B** left). Thus, the histogram of burst activation counts relative to Ras.GTP (**Fig. 3-8B, C** left) had to be normalized by the amount of time spent in each Ras.GTP bin (**τ**) (**Fig. 3-8B, C** right) to reveal the probability of SOS to achieve the processive activity state (**Fig. 3-7B, C,** see Methods).

The probability distributions showed that both SOS^{hdpc} and SOS^{FL} were more likely to enter the processive state as Ras.GTP levels increased (**Fig. 3-7B, C**), indicating that Ras.GTP provides allostery to SOS by enhancing the probability to achieve its hyperactive state. This supports previous single molecule measurements on SOS in reconstituted systems (39, 70) and agrees with recent findings that although the Grb2-binding domain inhibits allosteric site binding, SOS^{FL} is still able to fluctuate into the processive state (71). Both SOS^{hdpc} and SOS^{FL} exhibited a significant upsurge in probability to become hyperactive when Ras.GTP

levels reached 1000 molecules. This could point to a threshold above which SOS transforms analogue input signals into a digital outcome through potent Ras activation.

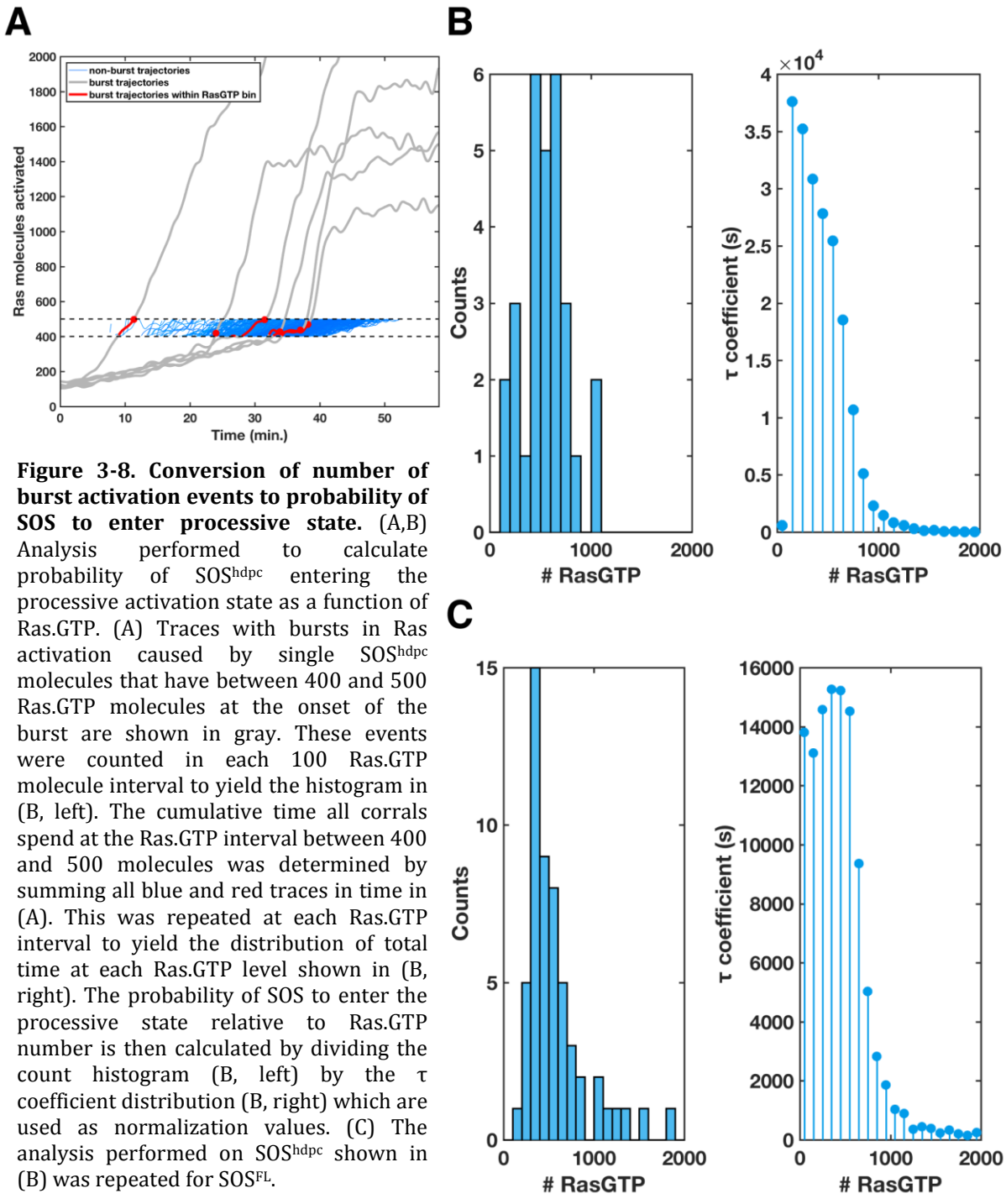

Figure 3-8. Conversion of number of burst activation events to probability of SOS to enter processive state. (A,B) Analysis performed to calculate probability of SOS^{hdpc} entering the processive activation state as a function of Ras.GTP. (A) Traces with bursts in Ras activation caused by single SOS^{hdpc} molecules that have between 400 and 500 Ras.GTP molecules at the onset of the burst are shown in gray. These events were counted in each 100 Ras.GTP molecule interval to yield the histogram in (B, left). The cumulative time all corrals spend at the Ras.GTP interval between 400 and 500 molecules was determined by summing all blue and red traces in time in (A). This was repeated at each Ras.GTP interval to yield the distribution of total time at each Ras.GTP level shown in (B, right). The probability of SOS to enter the processive state relative to Ras.GTP number is then calculated by dividing the count histogram (B, left) by the τ coefficient distribution (B, right) which are used as normalization values. (C) The analysis performed on SOS^{hdpc} shown in (B) was repeated for SOS^{FL}.

Single SOS molecules processively activate Ras despite GAP-catalyzed deactivation

In spite of autoinhibition by the PR domain, SOS^{FL} was still capable of processive Ras activation in the absence of receptor-dependent recruitment (**Fig. 3-6B, Fig. 3-7C**). This observation suggests that rapid Ras activation could spontaneously occur if no additional

mechanisms were in place to oppose SOS activity. Since Ras activation is tightly regulated by both GEFs and GAPs under physiological conditions (25, 129), we hypothesized that the addition of Ras-deactivating enzymes would provide the necessary balance to inhibit spurious Ras activation.

NF1-333 is the minimal functional domain of NF1 that has GTPase activity (130) and exhibited homogeneous first order Ras deactivation kinetics with a mean rate constant of 1.0×10^7 s^{-1} M^{-1} in the microarray assay measured using the RBD sensor (**Fig. 3-9**). With the knowledge that SOS has a mean catalytic rate constant 1600- to 3000-fold lower than that of NF1-333 without Ras.GTP priming (**Fig. 3-5A,B**), NF1-333 and SOS were added in ratios that enabled the rate of Ras deactivation to outcompete Ras activation by 40-fold. This condition was tested to determine the catalytic activities of SOS under conditions that suppressed Ras activation. 97% of the corrals exhibited minimal Ras activation with an average 2.5% of total available Ras activated at the endpoint. However, even in the presence of GAP activity, bursts in Ras activation was observed in a few corrals (**Fig. 3-10**), some with more than two bursts detected over the time-lapse. This showed that even in conditions where SOS allosteric activation was minimized by suppressing Ras.GTP production, SOS is capable of fluctuating into the processive state to cause rapid Ras activation.

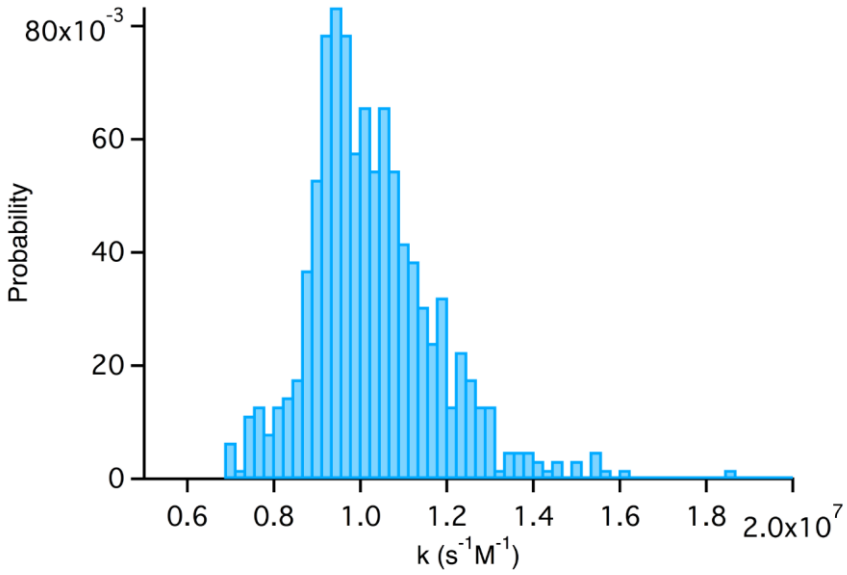

Figure 3-9. NF1-333 deactivates Ras homogeneously. Distribution of Ras deactivation rates catalyzed by 500 pM NF1-333 added to Ras.GTP-tethered SLBs. Measurements were made using the RBD sensor with 600 corrals simultaneously imaged.

The major effect of added deactivation catalysis is the decrease in amplitude of burst Ras activation. Observed continuous bursts in Ras.GTP production rarely activated more than 50% of total available Ras, and almost all faced immediate deactivation. Four of 600 imaged corrals reached a maximum activation level above 50% of total available Ras achieved through multiple burst phases. In addition, only two of the regions achieved full Ras activation. One notable observation is that bursts in Ras activation correlated with detection of stably recruited single SOS molecules, and Ras.GTP level decays as a single exponential immediately after the SOS molecule disappears (**Fig. 3-10**). These results indicate that GAP likely plays a role in causing processive, membrane-bound SOS to desorb back to solution. The data collectively shows that GAP-catalyzed Ras deactivation played a

significant role in suppressing processive Ras activation by SOS, but SOS was not completely inhibited from activating thousands of Ras in the minute timescale. This suggests that SOS under opposing deactivation pressure still requires additional mechanisms to prevent spontaneous burst Ras activation.

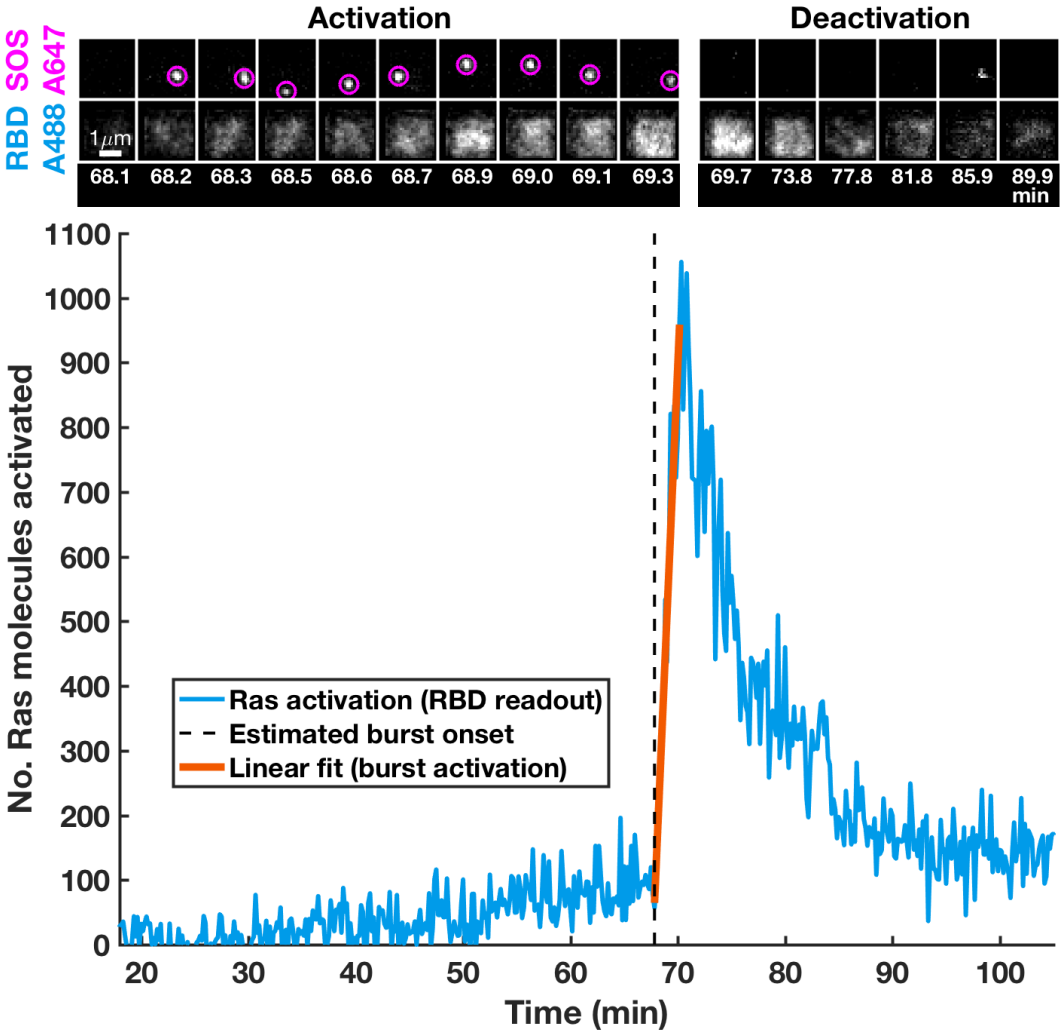

Figure 3-10. Single molecule SOS activates thousands of Ras processively despite added Ras deactivation activity by GAPs. TIRFM images of Alexa 647-labeled SOS^{hdpc} (top row) and fluorescent RBD sensor (bottom row) tracked in a single corral over 22 minutes starting at the onset of rapid Ras activation (dashed line). Identified single molecules of SOS are circled in pink. The number of Ras molecules activated in the corral between 20 and 105 minutes after SOS addition is plotted in blue, and the orange line marks the period of detected burst in Ras activation. Scale bar = 1 μm.

Discussion

SOS autoregulation by both its positive feedback loop and regulatory domains has been established by *in vitro* and *in vivo* measurements (35-38, 121, 123, 128). Positive feedback is manifested as increased catalysis and recruitment when the allosteric pocket of SOS is engaged with Ras.GTP (36, 38, 69, 70). Single molecule SOS studies in reconstituted systems demonstrated that a single allosterically activated protein can turnover thousands of Ras molecules over minutes (39, 70, 71). On the other hand, SOS activation is autoinhibited by its N- and C-terminal domains, which act independently to inhibit SOS membrane-recruitment (35, 36, 71, 72). These findings collectively show that single SOS molecules have the potential to activate Ras rapidly without receptor-mediated recruitment and, thus, require mechanisms to prevent hyperactivation. However, mysteries regarding SOS^{FL} activation and potentiation of Ras remain unknown. For example, the range of activity states achievable by SOS^{FL} that is initially autoinhibited has not been characterized. If multiple activity states exist, the structural configurations and impact on Ras signaling of each state have yet to be determined. These insights are only achievable through single molecule measurements on SOS^{FL} that can detect a broad range of catalytic activities.

Our data presents new insights into receptor-independent full-length SOS activation and its ability to overcome multilayer inhibition to activate Ras. Autoinhibited SOS can transition into two distinct active states: a transient state which activates Ras by brief interactions with the membrane (lasting <20 ms), and a processive state in which a stable, membrane-bound single molecule can activate thousands of Ras over minutes (**Fig. 3-11**). The findings

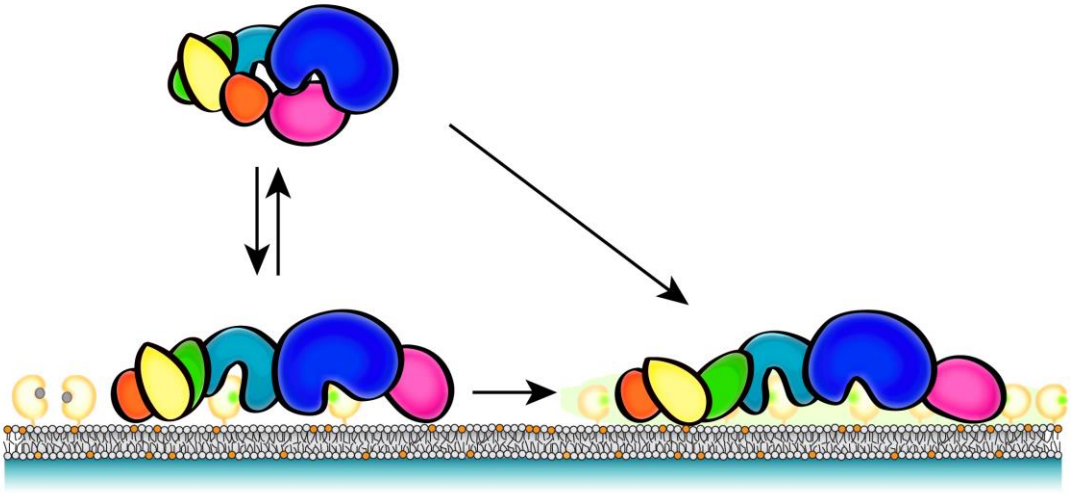

Figure 3-11. Model for SOS activation. N- and C-terminal regulatory domains act independently to autoinhibit SOS in the cytosol. In the absence of receptor stimulation, autoinhibition is released through interactions with negative lipids in the membrane in addition to stochastic fluctuations of the PR domain which enables dual-Ras binding at the catalytic and allosteric pockets. Release of PR domain autoinhibition without Grb2-mediated recruitment are rare but detectable. SOS engaged to two Ras molecules can be in the transient or processive activation modes. Both active forms of SOS interact with Ras at the allosteric pocket, which indicates the existence of structural differences between the two states.

demonstrated here argue that only the processive state is consequential in signal transduction. Transient state activity by SOS^{FL} was barely detectable on Ras bilayers and could be eliminated with the addition of low levels of GAP. Thus, the primary mode of SOS activation of Ras is through processive, single molecules, consistent with earlier studies (39, 70, 71). Despite autoinhibition from N- and C-terminal domains, SOS is capable of fluctuating into the processively active configuration without receptor-mediated recruitment.

We show that single molecule SOS^{FL} is allosterically activated by Ras.GTP through increased probability of transitioning from the inactive state to the processive state. Since the processive state is the only active form of SOS that generates measurable Ras activation under the presence of GAP activity, Ras.GTP-induced membrane recruitment is the key to SOS positive feedback. This finding is supported by experiments in which the number of stably recruited SOS molecules is significantly reduced when Ras.GTP production was suppressed by added GAPs. SOS catalysis is, however, unaffected by the nucleotide state. This confirms that Ras.GTP-mediated allosteric activation of SOS^{FL} is manifested as enhanced stable recruitment of SOS to the membrane, which, in turn, increases the overall activation of Ras (36, 70). Under complete autoinhibition from its regulatory domains, SOS still exhibits increased probability to transition to the processive state mediated by Ras.GTP. This suggests that SOS acts as an efficient analogue-to-digital Ras activator and that Ras.GTP must be kept at minimal levels to inhibit spontaneous SOS activation.

Structural differences between the transient and processive states of SOS are also elucidated. Since the catalytic pocket is insensitive to nucleotide state (53), changes in SOS catalysis induced by nucleotide identity are attributed to allosteric-Ras binding. Our study shows that SOS in the transient state undergoes a ten-fold increase in catalytic activity with Ras.GTP-priming, indicating that SOS engages Ras at the allosteric pocket. Processive SOS requires interactions with two Ras molecules (39, 70), which is further supported by measurements using the cdc25 domain of the GEF RasGRF1 in the Ras activation assay in which no burst activation events were observed (data not shown). These results prove that Ras binding at the catalytic site alone does not lead to processivity, but, instead, SOS requires interactions with two Ras molecules to exhibit any measurable activity consistent with structural data (38). Therefore, allosteric-Ras binding is not the defining factor that locks SOS in the processive state. Instead, SOS must experience other conformational changes on the membrane to transition between the two active states (**Fig. 3-11**). It would thus be informative to investigate possible structural configurations of SOS and small molecules that could limit domain flexibility of the protein. Alignment of four recent SOS^{cat} structures yield an RMSD value below 0.26, indicating that structural differences between the two active states of SOS can only be revealed if flanking regulatory domains are intact.

The question now shifts to how cells prevent aberrant Ras activation in the basal state given the potency of single SOS proteins. Our study provides evidence that GAP plays a major role in limiting SOS processivity by suppressing Ras.GTP production, which, in turn, reduces the probability of SOS to transition to the processive state. Furthermore, the intensity and duration of processive SOS activity are reduced upon GAP addition, indicating that GAPs likely act as competitive inhibitors. GAPs are expected to exist at higher

concentrations in the cell with more complex activity than the simple bimolecular kinetics provided by NF1-333. Though GAP autoregulation remains elusive, structural studies show that GAP activity is potentially modulated by membrane and small GTPase binding (28, 73, 131). Ras spatiotemporal regulation is another mechanism that would modulate SOS processivity. Ras dynamically cycles between plasma membrane and endomembranes, and its degree of clustering is constrained in terms of physical size and lifetime (56, 58, 132, 133). Certain proteins, such as PDEδ and calmodulin, have been shown to facilitate Ras redistribution in the cell (56, 134, 135). Thus, these processes can restrict Ras accessibility to membrane-bound SOS. Effector protein compartmentalization and autoregulation are also not explored in our study. For example, Raf is autoinhibited in the cytosol until it is recruited to the membrane by active Ras (42). It undergoes a series of phosphorylation events before Raf dimerization and activation (42). Only when all steps are met can Raf transmit signal from Ras.GTP to the rest of the MAPK cascade. All of the above mechanisms can thus work synergistically to restrict Ras activation by single processive SOS without receptor stimulation.

Materials

The lipids used to make SLBs were: (L-α-phosphatidylcholine (Egg, Chicken), Egg-PC; L-α-phosphatidylinositol-4,5-bisphosphate (Brain, Porcine), PIP_2; 1,2-dioleoyl-sn-glycero-3-phosphoethanolamine-N-[4-(p-maleimidomethyl)cyclohexane-carboxamide], MCC-DOPE) (Avanti Polar Lipids, Alabaster, AL). The nucleotides used were: guanosine triphosphate (GTP), guanosine diphosphate (GDP), and guanosine 5′-[β,γ-imido]triphosphate (GppNHp) (Sigma-Aldrich, St. Louis, MO). Imaging buffer consisted of 10 mM β-mercaptoethanol (BME), 20 mM glucose, 2mM Trolox, 0.32 mg/mL glucose oxidase, 0.05 mg/mL catalase, and 0.02 mg/mL β-caesin, all from Sigma-Aldrich except glucose oxidase (Serva Electrophoresis, Heidelberg, Germany).

Methods

Protein purification and labeling

H-Ras (1-181, C118S) (human H-Ras protein with residues 1-181 and a point mutation to serine at residue C118 hereafter termed Ras), SOS^{cat} Cys-lite (566-1049, C838A, C635A, C980S, and E718C), SOS^{hdpc} (1-1049), and the GTPase activation (GAP) domain of NF1 (1198-1530), termed NF1-333, were expressed and purified based on the protocols described in previous work (36, 40). Briefly, Ras plasmid was cloned into pET-20b vector using Nde1 and Xho1 restriction sites, then transformed into Escherichia coli cells (Rosetta DE3) (Novagen, Darmstadt, Germany). Cells were lysed (50 mM Na_2HPO_4 (pH 8.0), 300 mM NaCl, 0.4 mM BME, 1 mM PMSF, and DNase) and recirculated over HiTrap (Co^{2+}) column. Protein was eluted with a linear gradient of 50 mM Na_2HPO_4 (pH 8.0), 300 mM NaCl, 0.4 mM BME, 500 mM imidazole and desalted overnight at 4 ^oC in 4 L of 50 mM Na_2HPO_4 (pH 8.0), 300 mM NaCl, and 0.4 mM BME with tobacco etch virus (TEV) protease (Sigma-Aldrich, St. Louis, MO) incubation. After a second HiTrap (Co^{2+}) column recirculation, protein was concentrated and gel-filtered using Superdex75 column in 20 mM Tris (pH 8.0, 200 mM NaCl, 5 mM $MgCl_2$, 1 mM TCEP, 10 uM GDP). Appropriate fractions were pooled and concentrated to ~5 mg/mL then frozen for storage.

NF1-333 plasmid from MGC human NF1 Sequence-Verified cDNA (Clone ID: 9053174) (Dharmacon, Lafayette, CO) was cloned into a vector containing his6-GST-TEV (Macrolab, Berkeley, CA) using ligation independent cloning. The protein was expressed and purified identically to Ras except a Gluthathione column was used to cleave the N-terminal GST-tag prior to gel filtration chromatography.

SOS plasmids, provided by J. Kuriyan, were expressed in Escherichia coli cells (BL21 DE3) (Novagen, Darmstadt, Germany). Cells were lysed in 25 mM Tris (pH 7.5), 500 mM NaCl, 0.4 mM BME, 1 mM PMSF, and DNase, and recirculated over HiTrap (Co^{2+}) column equilibrated in 25 mM Tris (pH 7.5), 500 mM NaCl, and 0.4 mM BME. Protein was eluted with a linear gradient of in 25 mM Tris (pH 7.5), 500 mM NaCl, 0.4 mM BME, and 500 mM imidazole before TEV protease treatment and dialysis in 4L of 25 mM Tris (pH 7.0), 300 mM NaCl, and 0.4 mM BME overnight at 4 ^oC. Cleaved His-tag was removed with HiTrap (Co^{2+}) recirculation, and collected protein was concentrated in 25 mM Tris (pH 7.5), 50 mM NaCl,

1 mM TCEP and loaded onto MonoQ HP column. Protein was eluted with a linear gradient of 25 mM Tris (pH 7.5), 500 mM NaCl, 1 mM TCEP, concentrated, and gel-filtered using Superdex200 in 25 mM Tris (pH 7.5), 100 mM NaCl, 1 mM TCEP. 10% glycerol was added before further concentration and frozen before storage.

SOS^{hdpc} was labeled with Alexa Fluor 647 maleimide (Thermo Fisher Scientific, Waltham, MA) using a 1:2 reaction at room temperature. 100 mM BME was added 30 minutes after for an additional 10 minutes. Excess dye was removed using centrifugation filters and the labeled protein was gel filtered. Labeling efficiency was determined to be 80% using UV-vis spectroscopy (NanoDrop 2000, Thermo Scientific).

Ras activation sensor purification and labeling

MGC human Raf-1 Sequence-Verified cDNA (Clone ID: 3904404), henceforth referred to as CRaf, was purchased from Dharmacon. The Ras-binding domain (RBD) of CRaf was PCR-amplified with Kpn1 and Not1 restriction sites flanking its N-terminus and C-terminus respectively. The sequence was cloned into a modified pETM-33 parent vector with an inserted SNAP-tag after the N-terminal his6-GST-3C site. A K65E point mutation of RBD was added using site-directed mutagenesis.

The SNAP-tagged Ras binding domain (RBD) K65E of CRaf, hereafter termed SNAP-RBD, was purified identically to Ras as described in the previous section with minor changes (40). PreScission protease was used to cleave off the 3C site adjacent to the N-terminus of RBD. The protein was recirculated over HiTrap (Co^{2+}) and Gluthathione columns subsequently to remove His6-GST and GST-PreScission tags respectively before gel filtration chromatography.

SNAP-RBD was mixed with SNAP-Surface Alexa Fluor 488 (New England BioLabs, Ipswich, MA) at a 1:1.5 reaction in PBS and 10 mM DTT at 18°C overnight. The solution was diluted in 20 mM Tris, 200 mM NaCl, 10% glycerol, and 1 mM TCEP before concentration and gel filtration. The labeling efficiency was 64.4% determined by UV-vis spectroscopy (NanoDrop 2000, Thermo Scientific).

Preparation of Ras-functionalized supported lipid bilayers

Supported lipid bilayers (SLBs) functionalized with Ras was prepared based on methods described previously (39, 59). Briefly, glass substrates were cleaned in 2% Hellmanex III solution (Hellma Analytics, Müllheim, Germany). They were sonicated in a 50:50 isopropanol (IPA): Milli-Q water (H_2O) mixture and H_2O for 15 minutes in each step. Glass substrates were etched in piranha solution (3:1 mixture of H_2SO_4: H_2O_2) for 5 minutes, rinsed with H_2O, and adhered to sticky-Slide $VI^{0.4}$ open channel slides (Ibidi, Martinsried, Germany). A lipid mixture of 94% Egg-PC, 3% PIP_2, and 3% MCC-DOPE in chloroform was rotorvapped and placed under nitrogen gas for 20 minutes. Dried lipid films were rehydrated in PBS to form a 1 mg/mL solution, which was extruded 15 times through a 30 nm pore-sized polycarbonate filter (EMD Millipore, Billerica, MA) to create small unilamellar vesicles (SUVs) before diluting to 0.5 mg/mL. SUVs were deposited in the assembled ibidi chambers and incubated for 30 minutes to form bilayers. 2 mg/mL β-caesin and 0.4 mg/mL Ras diluted in PBS were added subsequently to the SLBs and

incubated for 10 minutes and 2.5 hours respectively. Unreacted maleimide-modified lipid head groups were reduced after a 10 minute incubation in 5 mM BME. PBS buffer was exchanged to reaction buffer (40 mM HEPES, 100 mM NaCl, and 5 mM $MgCl_2$, pH 7.4). Samples were stored overnight at 4°C in 5 μM GDP diluted in reaction buffer, and were allowed to equilibrate to room temperature the next day before image acquisition.

Optical microscopy

Images were acquired using total internal reflection fluorescence microscopy (TIRFM) on a Nikon Eclipse Ti inverted microscope with 100X oil immersion TIRF objective with 1.49 NA and an Andor iXon EMCCD camera. 488, 561, and 637 nm lasers from Coherent were used as illumination sources. The following filter sets were used for imaging: ET500LP and ET525/50M for 488 nm channel, ET575LP and ET600/50M for 561 nm channel, and ET660LP and 700/75M for 637 nm channel. The microscope was controlled using μManager (136) and aligned to produce Koehler illumination.

Characterization of RBD sensor as Ras activation readout

The fluorescently labeled RBD sensor was characterized using three approaches: 1) calibration between fluorescence intensity and Ras.GTP density, 2) sensor equilibration kinetics, and 3) sensitivity to Ras activation and deactivation by SOS^{cat} and NF1-333 respectively.

RBD sensor intensity conversion to Ras.GTP level was calibrated using Ras-functionalized SLBs prepared on glass slides with Ras concentrations between 0.05 and 0.6 mg/mL. After BME incubation, Ras was loaded with 5 μM GppNp-Atto488 using 20 nM SOS^{cat} in reaction buffer to catalyze nucleotide exchange for a minimum of 10 minutes. Samples were washed with 1 mL of 10 mM BME in reaction buffer immediately before fluorescence correlation spectroscopy (FCS) measurements. Samples were washed with 2 mL reaction buffer and bound nucleotide was exchanged to unlabeled GTP in a 10-minute incubation with 1 mM GTP and 20 nM SOS^{cat} Cys-Lite. Background fluorescence was measured using TIRFM after samples were rinsed with 2 mL reaction buffer. Images were acquired 5 minutes after injection of 50 nM of RBD sensor in IB. Intensities of all images per sample were averaged after subtraction of background fluorescence and plotted against the measured Ras density to produce the calibration curve (**Fig. 3-2A**).

Equilibration kinetics of the sensor was measured by acquiring 5 s to 10 s time-lapses (n=3) of Ras-decorated SLB (as described above) with the addition of 25 nM – 50 nM sensor diluted in IB. Excess solution in the sample chamber was removed immediately after injection. Ras.GppNp density was approximately 1000 molecules/ μm^2 obtained from the calibration curve. Each plotted trace was normalized to the maximum intensity (**Fig. 3-2B**).

RBD sensor sensitivity to GEF-activation and GAP-deactivation of Ras was measured on Ras-functionalized SLBs. 5 nM Alexa Fluor 647 labeled SOS^{cat}, 25 nM RBD sensor, and 1 mM GTP in IB was added to Ras.GDP SLB equilibrated in 25 nM sensor (**Fig. 3-2C**). In a different sample, Ras.GTP SLB was equilibrated in 25 nM sensor before injection of 1 nM NF1-333 and 25 nM RBD sensor (**Fig. 3-2D**). 3 s time-lapse measurements were acquired in each condition.

Ras activation microarray assay with single SOS imaging

Ras-tethered SLBs prepared the previous day was equilibrated to room temperature. In experiments that evaluated effects of Ras.GTP on SOS catalytic activity, an additional nucleotide exchange step was performed. These samples were washed with 2 mL of stripping buffer (40 mM HEPES and 150 mM NaCl) and incubated in 50mM EDTA, 40 mM HEPES, 150 mM NaCl for 20 minutes. They were washed with another 2 mL of stripping buffer before addition of 100 uM of GDP or GTP in reaction buffer. All samples were washed with 2 mL of reaction buffer before imaging.

Images were acquired before and 5 minutes after the addition of 50 nM RBD sensor in IB into the sample to measure background fluorescence and starting Ras.GTP density. 50 nM RBD sensor, 1 mM GTP, and SOS^{hdpc} or SOS^{FL} between 1 and 50 nM in IB was added at the beginning of time-lapse acquisition. In conditions where deactivation pressure from GAPs were tested, 500 pM of NF1-333 was added concurrently with SOS. Alexa488-RBD sensor was imaged every 10 or 20 s, and SOS^{hdpc}-Alexa647 or SOS^{FL}-Alexa555 was imaged simultaneously every 1 to 10 s for 30 to 60 minutes. The total Ras density in each corral was measured at the end of the time-lapse after a 5-minute incubation of 20 nM SOS^{cat} and 1 mM GTP in reaction buffer and addition of 50 nM RBD sensor in IB to fully activate all Ras molecules.

Kinetic rate equations

In the absence of GEFs, the rate at which Ras.GTP density $\mathbf{X_{Ras.GTP}}$ increases due to passive exchange of bound GDP to GTP from solution is described as:

$$\frac{\mathbf{dX_{Ras.GTP}}}{\mathbf{dt}} = \mathbf{k_i X_{Ras.GDP}} \qquad \textbf{[3-1]}$$

Where $\mathbf{X_{Ras.GDP}}$ represents Ras.GDP density, $\mathbf{k_i}$ is the intrinsic nucleotide exchange rate constant, and $\mathbf{t}$ is time. Upon addition of SOS at concentration $\mathbf{X_{SOS}}$, the rate of Ras.GTP production in traces with no burst in Ras activation is:

$$\frac{\mathbf{dX_{Ras.GTP}}}{\mathbf{dt}} = (\mathbf{k_i} + \mathbf{k_{eff} X_{SOS}})\mathbf{X_{Ras.GDP}} \qquad \textbf{[3-2]}$$

Where $\mathbf{k_{eff}}$ represents the effective catalytic rate constant of SOS in the transient state. In the scenario where a single SOS molecule in the processive state is stably recruited to the membrane, the rate of Ras activation is:

$$\frac{\mathbf{dX_{Ras.GTP}}}{\mathbf{dt}} = (\mathbf{k_i} + \mathbf{k_{eff} X_{SOS}} + \mathbf{k'})\mathbf{X_{Ras.GDP}} \qquad \textbf{[3-3]}$$

Where $\mathbf{k'}$ is the rate at which a single SOS turns over Ras molecules.

Image processing
Background intensity subtraction and field illumination correction were performed on the TIRFM images using ImageJ. Custom code on Matlab was used to identify the chromium grid that segments the SLB and to generate coordinates of each corralled region. Fluorescence intensities of the regions at each time point were extracted using DipImage and converted to number of Ras activated (**Fig. 3-2A**).

Effective catalytic rate constant analysis
Ras.GTP values measured 10 min after SOS addition allowed clear differentiation between corrals that experienced burst activation from those that did not at or before this selected time point. The distribution of Ras.GTP numbers at 10 min is shown in **Figure 3-6C**. Ras activation traces from corrals with Ras.GTP level below the mean plus two times the standard deviation ($\boldsymbol{\mu + 2\sigma}$) with no identified change points at 10 min were plotted (**Fig. 3-6A, B** narrow plots). These traces were then used to compute the effective catalytic rate constant ($\mathbf{k_{eff}}$) of SOS using **Equation 3-2**.

Calculation of the probability of SOS to enter processive state
Corrals were determined to experience bursts in Ras activation if two or more change points in the intensity traces were identified. Ras.GTP level was segmented into 100 molecule intervals, and the number of Ras.GTP at the onset of each burst activation was determined (**Fig. 3-7A**, red dots). Histograms of burst activation events that occur in each interval was summed and plotted as a function of Ras.GTP for both SOS^{hdpc} (**Fig. 3-8B** left) and SOS^{FL} (**Fig. 3-8C** left). These distributions were normalized by the cumulative time (τ) spent by all corrals at each Ras.GTP interval (**Fig. 3-8B, C** right). The resulting distributions yield the probability of the two SOS constructs to transition to the processive state relative to Ras.GTP number using the equation:

$$\mathrm{P(processive\ SOS\ observed\ in\ Ras.GTP} = [\mathrm{x}, \mathrm{x} + \Delta)) = \frac{\#\ \text{burst events in } [\mathrm{x}, \mathrm{x} + \Delta)}{\tau[\mathrm{x}, \mathrm{x} + \Delta)} \qquad \textbf{[3-4]}$$

Where Δ is 100 and $\mathbf{x}$ is an arbitrary Ras.GTP value. An example of this calculation is illustrated for one data set that studied SOS^{hdpc} at Ras.GTP = [400,500). Six burst activation events were identified in this Ras.GTP bin (**Fig. 3-8A**). τ[400,500) was computed by summing the time taken for each trace to transit across that particular Ras.GTP interval (all blue traces plus the red traces). The probability to transition to the processive state within Ras.GTP = [400,500) was then calculated by dividing the six burst events by τ[400,500). This process was repeated for each Ras.GTP interval to generate the full distributions (**Fig. 3-7B,C**).

Summary of findings

The findings of this dissertation contribute to our understanding of Ras spatial organization and activation in the membrane environment. Molecular oxygen mediates protein radicalization and subsequent crosslinking, which, in this case, provides a mechanism for Ras to form covalent dimers and higher order oligomers. Dityrosine bonding is one dimerization motif and since Ras has a high concentration of surface exposed tyrosines, it renders Ras especially sensitive to dimerization. The photosensitization reactions performed on supported membranes are likely to reflect physiological oxidative stress induced by reactive oxygen species, which implies that Ras dimers and oligomers can exist under physiological conditions.

As for Ras activation by its key regulator SOS, two distinct activity states were observed: a transient state with low catalytic rate, and a processive state that induces rapid Ras.GTP production. Despite autoinhibition from N- and C-terminal domains, full-length SOS is capable of activating Ras processively. In addition, Ras.GTP mediates SOS activation by enhancing the probability for single molecules of SOS to transition to the hyperactive state. Since Ras activation by SOS with transient activity is easily eliminated with low levels of GTPase activating proteins, the primary mode of Ras activation by SOS is through single processive enzymes. This indicates that single SOS molecules are consequential in Ras signaling, and that additional measures must be in place to prevent spurious Ras activation without receptor stimulation.

Future directions

While the work in this dissertation elucidates a handful of mechanisms that regulate Ras signaling, many more have yet to be uncovered to provide a holistic picture of Ras signal propagation in the physiological context. For example, it remains unclear if Ras dimer formation are primarily driven by Ras itself or its binding partners in the cell context, and if Ras dimers are necessary for downstream signaling. As for SOS-mediated Ras activation, the existence of processive SOS molecules that rapidly activate Ras has yet to be confirmed in live cells. If SOS can indeed access such a hyperactive state, the downstream consequences of local bursts in Ras activation are elusive. Although these questions remain unanswered, there are many experiments that can be done in the near future to advance our understanding in these areas. The rest of this chapter will focus on future experiments, which can be performed using our current expertise, to further our knowledge on mechanisms that govern Ras signaling.

Future Ras dimerization studies

Although H-Ras does not intrinsically form dimers at surface densities below 1000/μm^2 in the absence of oxidation reactions as shown in Chapter 2, there are three additional Ras

isoforms, each with a different set of chemical cues for membrane localization (26). For example, K-Ras-4B contains a polybasic chain in the hypervariable region (HVR) with a C-terminal farnesyl lipid tail whereas H-Ras contains two palmitoyl and one farnesyl lipid groups near the C-terminus (26). Therefore, it would be informative to understand the potential for each isoform to intrinsically form dimers and higher order oligomers using constructs that preserve the native lipid moieties. Our lab recently started a collaboration with the National Cancer Institute (NCI) with protein experts who can purify Ras constructs with intact, native lipid domains. Thus, studying these proteins on supported membranes will allow us to determine if Ras dimerization potential is mediated by Ras membrane-binding signals. Of course, membrane composition can potentially mediate dimer formation of the various Ras isoforms. There had been many studies from John F. Hancock's lab that imaged Ras clustering and lipid colocalization on fixed plasma membranes (PMs) using electron microscopy. Recent data indicated that K-Ras-4B preferentially binds phosphatidylserine (PS) lipids over PIP_2 or any other lipids, yet mutating parts of the polybasic HVR affects its colocalization with PS headgroups (137). These measurements suggest that lipids modulate isoform-specific Ras spatial organization. It would therefore be interesting to determine if Ras can form dimers on supported membranes by varying the lipid composition while keeping Ras densities at physiological levels.

Other parameters which can affect Ras dimer formation are Ras activation state as well as the addition of binding partners. Ras dimerization dependence on nucleotide state can be easily tested on the SLB platform by incubating Ras with fluorescently labeled GDP or GTP. There is an abundance of Ras binding partners that can be tested, but the most promising candidate is Raf. Studies have shown that Raf dimerizes via the kinase domain (62, 63), and recent observations from crystal structure studies in Carla Mattos' lab indicate that Ras binding to the RBD of Raf alone can lead to dimer formation (data not published). Thus, one can test if active Ras can form dimers upon RBD interactions on the SLB platform. Ras dimerization induced by full-length Raf can also be tested on the same platform by extracting Raf proteins from whole cell lysates and applying it on Ras-functionalized SLBs demonstrated in Lee et al. 2017. If Raf RBD binding to Ras induces Ras dimerization, the RBD of phosphoinositide 3-kinase (PI3K) can also be examined.

The most definitive test to determine if Ras has the intrinsic properties to form dimers is to find point mutations that can alter the degree of dimer formation. Given the observed Ras dimer interfaces from *in silico* models and crystal structures (68, 138), one can mutate amino acids at the surface hypothesized to induce or inhibit Ras dimerization. Many mutations can be created along the dimer interface, so a high throughput method to determine if there are any observable effects on Ras clustering at first pass would be ideal. Ras-functionalized on bilayers can be labeled using fluorescent nucleotides that act as FRET pairs, for example Atto488 and Atto565, and FRET efficiency can be measured for each Ras mutant. Alternatively, the same measurements can be performed using Ras tethered to bilayer-coated glass beads for more rapid determination. Only the mutations that lead to changes in FRET efficiency should then be examined more closely using FCS to determine if Ras dimerization is indeed affected.

If Ras dimers are identified from the above measurements, its effect on Ras signaling can be investigated in cells. Mouse embryonic fibroblasts (MEFs), which can be rendered Rasless upon exposure to 4-hydroxytamoxifen, had been developed recently (139). These cells can thus be transfected with labeled Ras that are determined to affect Ras dimerization from the proposed *in vitro* measurements. The degree of Ras dimerization can be verified using fluorescence microscopy techniques, and downstream signaling effects, for example on MEK and ERK activation, can be measured by performing Western blot analysis. The cells can also be co-transfected with labeled ERK so that its translocation to the nucleus will provide a more direct readout of its activation (140).

Future single molecule SOS studies

The results from single molecule SOS studies using the *in vitro* Ras activation assay in Chapter 3 suggests that SOS primarily activates Ras in the processive state by single enzymes. The next step would be to confirm if SOS can access the processive activation state in cells. This involves co-transfecting cells with labeled SOS and labeled, real-time Ras activation sensor. Since the goal is to measure Ras activation by single SOS molecules, SOS can be transfected at low levels through careful selection of the promoter and can be labeled with mEOS2, which is a green-to-red photoconvertible dye suited for single molecule imaging (141). The transfection of labeled SOS can also be performed in SOS-deficient DT40 B cells in order to only assess the effects of transfected SOS (70). Since processive SOS molecules activate Ras rapidly *in vitro*, the cellular Ras activation sensor must provide a quantifiable readout of Ras.GTP levels with second resolution at the site of activation. Multiple strategies exist to monitor Ras activation in cells (142-144), so these methods can be evaluated to determine if they allow quantitative measurements of Ras.GTP levels at the necessary spatiotemporal resolution. Opto-SOS, an optogenetics tool developed by Jared. E. Toettcher that recruits SOS to the PM with 650 nm wavelength illumination (145), can be co-transfected with the Ras activation sensor to determine the effectiveness of the sensor on detecting rapid, localized Ras.GTP production. The collective use of these tools would allow SOS activity states to be measured in cells and the existence of processive SOS to be determined.

In addition to Ras activation, downstream signaling effects of SOS catalysis can be evaluated concurrently. Labeled ERK can be co-transfected in cells along with the proteins discussed in the paragraph above so that its translocation to the nucleus will serve as a readout for its activation. Assessing both immediate and downstream effects of PM-recruited SOS would provide a more complete picture on the input-outcome response of SOS-catalyzed Ras activation.

Single molecule SOS studies have primarily focused on SOS catalysis without receptor-mediated membrane-recruitment, but its signaling effects under receptor-stimulated conditions are also important. Current efforts are underway in our lab to evaluate SOS activity when adaptor molecules are available for SOS binding via the C-terminal PR domain. These experiments can be extended to determine SOS catalysis with receptor-stimulation in cells to compare to basal state conditions when receptors are not activated

by growth factors. This would provide information on whether signals from SOS-catalyzed Ras activation are processed differently under activated and non-activated conditions to generate cellular outcomes.

One of the main conclusions in the study in Chapter 3 is that SOS has two active forms, both of which bind to two Ras molecules. It would therefore be interesting to determine the structural differences between the two states, which would provide insights for targeting SOS that could prevent its transition to the hyperactive state. These active states of SOS are only accessible if SOS is anchored to the membrane, so crystallographic studies would be difficult to uncover such structures even if purified full-length SOS were readily available. However, cryo-electron microscopy presents an increasingly powerful imaging technique that can resolve membrane protein structures on native membranes (146), so it presents a potential avenue to resolve subtle structural variations between the two active forms of SOS.

Last but not least, sustained ERK activation oscillations have been observed *in vitro* and *in vivo* and appear to affect the rate of cellular proliferation (147-149). This phenomenon is recapitulated *in silico* when negative feedback loops and intrinsic ultrasensitivity in MAPK cascade are incorporated in the model (150). Preliminary data from our lab show that Ras samples with SOS and NF1-333 maintained at constant concentrations within a specific range produced oscillatory Ras.GTP production (**Fig. 4-1**). This observation indicates that competing activities of SOS and GAPs alone could lead to oscillations in the activation of Ras and possibly proteins downstream in the MAPK cascade. It would therefore be interesting to investigate how the amplitude and frequency of these oscillations can be modulated *in vitro* and extend these manipulations to live cell studies.

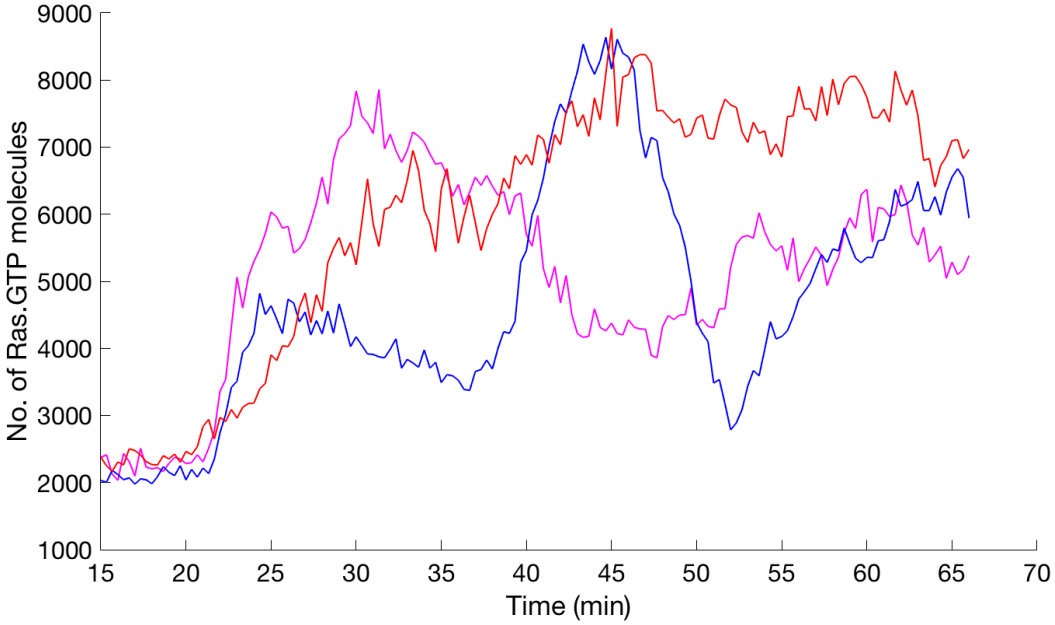

Figure 4-1. Ras activation displays oscillatory behavior with the addition of SOS and NF1-333. Example traces from three corrals that show oscillations in Ras.GTP production taken over the course of an hour.

5. References

1. J. T. Groves, J. Kuriyan, Molecular mechanisms in signal transduction at the membrane. Nature structural & molecular biology **17**, 659-665 (2010).
2. D. Lingwood, K. Simons, Lipid rafts as a membrane-organizing principle. Science **327**, 46-50 (2010).
3. B. N. Kholodenko, J. B. Hoek, H. V. Westerhoff, Why cytoplasmic signalling proteins should be recruited to cell membranes. Trends in cell biology **10**, 173-178 (2000).
4. J. Kuriyan, D. Eisenberg, The origin of protein interactions and allostery in colocalization. Nature **450**, 983-990 (2007).
5. S. L. Veatch et al., Critical fluctuations in plasma membrane vesicles. ACS Chem Biol **3**, 287-293 (2008).
6. A. R. Honerkamp-Smith, S. L. Veatch, S. L. Keller, An introduction to critical points for biophysicists; observations of compositional heterogeneity in lipid membranes. Biochimica et biophysica acta **1788**, 53-63 (2009).
7. M. P. Sheetz, Cell control by membrane-cytoskeleton adhesion. Nature reviews. Molecular cell biology **2**, 392-396 (2001).
8. C. R. Monks, B. A. Freiberg, H. Kupfer, N. Sciaky, A. Kupfer, Three-dimensional segregation of supramolecular activation clusters in T cells. Nature **395**, 82-86 (1998).
9. S. K. Bromley et al., The immunological synapse and CD28-CD80 interactions. Nat Immunol **2**, 1159-1166 (2001).
10. S. K. Bromley et al., The immunological synapse. Annual review of immunology **19**, 375-396 (2001).
11. J. B. Huppa et al., TCR-peptide-MHC interactions in situ show accelerated kinetics and increased affinity. Nature **463**, 963-967 (2010).
12. J. Huang et al., The kinetics of two-dimensional TCR and pMHC interactions determine T-cell responsiveness. Nature **464**, 932-936 (2010).
13. B. A. Freiberg et al., Staging and resetting T cell activation in SMACs. Nat Immunol **3**, 911-917 (2002).
14. V. Vogel, M. Sheetz, Local force and geometry sensing regulate cell functions. Nature reviews. Molecular cell biology **7**, 265-275 (2006).
15. M. J. Paszek et al., The cancer glycocalyx mechanically primes integrin-mediated growth and survival. Nature **511**, 319-325 (2014).
16. J. M. Shields, K. Pruitt, A. McFall, A. Shaub, C. J. Der, Understanding Ras: 'it ain't over 'til it's over'. Trends in cell biology **10**, 147-154 (2000).
17. M. Malumbres, M. Barbacid, RAS oncogenes: the first 30 years. Nature reviews. Cancer **3**, 459-465 (2003).
18. A. D. Cox, C. J. Der, The dark side of Ras: regulation of apoptosis. Oncogene **22**, 8999-9006 (2003).
19. M. E. Katz, F. McCormick, Signal transduction from multiple Ras effectors. Curr Opin Genet Dev **7**, 75-79 (1997).
20. Y. Pylayeva-Gupta, E. Grabocka, D. Bar-Sagi, RAS oncogenes: weaving a tumorigenic web. Nature reviews. Cancer **11**, 761-774 (2011).

21. A. D. Cox, S. W. Fesik, A. C. Kimmelman, J. Luo, C. J. Der, Drugging the undruggable RAS: Mission possible? Nature reviews. Drug discovery **13**, 828-851 (2014).
22. B. Papke, C. J. Der, Drugging RAS: Know the enemy. Science **355**, 1158-1163 (2017).
23. K. Wennerberg, K. L. Rossman, C. J. Der, The Ras superfamily at a glance. Journal of cell science **118**, 843-846 (2005).
24. I. R. Vetter, A. Wittinghofer, The guanine nucleotide-binding switch in three dimensions. Science **294**, 1299-1304 (2001).
25. A. G. Stephen, D. Esposito, R. K. Bagni, F. McCormick, Dragging Ras Back in the Ring. Cancer cell **25**, 272-281 (2014).
26. J. Spiegel, P. M. Cromm, G. Zimmermann, T. N. Grossmann, H. Waldmann, Small-molecule modulation of Ras signaling. Nature chemical biology **10**, 613-622 (2014).
27. D. Abankwa, A. A. Gorfe, J. F. Hancock, Mechanisms of Ras membrane organization and signaling: Ras on a rocker. Cell cycle **7**, 2667-2673 (2008).
28. J. Cherfils, M. Zeghouf, Regulation of small GTPases by GEFs, GAPs, and GDIs. Physiol Rev **93**, 269-309 (2013).
29. J. L. Bos, H. Rehmann, A. Wittinghofer, GEFs and GAPs: critical elements in the control of small G proteins. Cell **129**, 865-877 (2007).
30. J. Downward, Targeting ras signalling pathways in cancer therapy. Nature Reviews Cancer **3**, 11-22 (2003).
31. E. Porfiri, F. McCormick, Regulation of epidermal growth factor receptor signaling by phosphorylation of the ras exchange factor hSOS1. The Journal of biological chemistry **271**, 5871-5877 (1996).
32. L. Buday, J. Downward, Epidermal growth factor regulates the exchange rate of guanine nucleotides on p21ras in fibroblasts. Molecular and cellular biology **13**, 1903-1910 (1993).
33. A. M. Cheng et al., Mammalian Grb2 regulates multiple steps in embryonic development and malignant transformation. Cell **95**, 793-803 (1998).
34. G. M. Findlay et al., Interaction domains of Sos1/Grb2 are finely tuned for cooperative control of embryonic stem cell fate. Cell **152**, 1008-1020 (2013).
35. X. Qian, W. C. Vass, A. G. Papageorge, P. H. Anborgh, D. R. Lowy, N terminus of Sos1 Ras exchange factor: critical roles for the Dbl and pleckstrin homology domains. Molecular and cellular biology **18**, 771-778 (1998).
36. H. Sondermann et al., Structural analysis of autoinhibition in the Ras activator Son of sevenless. Cell **119**, 393-405 (2004).
37. S. Corbalan-Garcia, S. M. Margarit, D. Galron, S. S. Yang, D. Bar-Sagi, Regulation of Sos activity by intramolecular interactions. Molecular and cellular biology **18**, 880-886 (1998).
38. S. M. Margarit et al., Structural evidence for feedback activation by Ras.GTP of the Ras-specific nucleotide exchange factor SOS. Cell **112**, 685-695 (2003).
39. L. Iversen et al., Ras activation by SOS: allosteric regulation by altered fluctuation dynamics. Science **345**, 50-54 (2014).
40. J. Gureasko et al., Membrane-dependent signal integration by the Ras activator Son of sevenless. Nature structural & molecular biology **15**, 452-461 (2008).
41. T. D. Bunney et al., Structural and mechanistic insights into ras association domains of phospholipase C epsilon. Molecular cell **21**, 495-507 (2006).

42. H. Lavoie, M. Therrien, Regulation of RAF protein kinases in ERK signalling. Nature reviews. Molecular cell biology **16**, 281-298 (2015).
43. I. A. Prior, P. D. Lewis, C. Mattos, A comprehensive survey of Ras mutations in cancer. Cancer research **72**, 2457-2467 (2012).
44. A. B. Walsh, D. Bar-Sagi, Differential activation of the Rac pathway by Ha-Ras and K-Ras. The Journal of biological chemistry **276**, 15609-15615 (2001).
45. J. Yan, S. Roy, A. Apolloni, A. Lane, J. F. Hancock, Ras isoforms vary in their ability to activate Raf-1 and phosphoinositide 3-kinase. The Journal of biological chemistry **273**, 24052-24056 (1998).
46. J. K. Voice, R. L. Klemke, A. Le, J. H. Jackson, Four Human Ras Homologs Differ in Their Abilities to Activate Raf-1, Induce Transformation, and Stimulate Cell Motility. Journal of Biological Chemistry **274**, 17164-17170 (1999).
47. M. P. Quinlan, S. E. Quatela, M. R. Philips, J. Settleman, Activated Kras, but not Hras or Nras, may initiate tumors of endodermal origin via stem cell expansion. Molecular and cellular biology **28**, 2659-2674 (2008).
48. A. D. Cox, C. J. Der, Ras history: The saga continues. Small GTPases **1**, 2-27 (2010).
49. B. M. Willumsen, A. Christensen, N. L. Hubbert, A. G. Papageorge, D. R. Lowy, The p21 ras C-terminus is required for transformation and membrane association. Nature **310**, 583-586 (1984).
50. E. F. Pai et al., Structure of the guanine-nucleotide-binding domain of the Ha-ras oncogene product p21 in the triphosphate conformation. Nature **341**, 209-214 (1989).
51. A. B. Vojtek, S. M. Hollenberg, J. A. Cooper, Mammalian Ras interacts directly with the serine/threonine kinase Raf. Cell **74**, 205-214 (1993).
52. K. Scheffzek et al., The Ras-RasGAP complex: structural basis for GTPase activation and its loss in oncogenic Ras mutants. Science **277**, 333-338 (1997).
53. P. A. Boriack-Sjodin, S. M. Margarit, D. Bar-Sagi, J. Kuriyan, The structural basis of the activation of Ras by Sos. Nature **394**, 337-343 (1998).
54. J. F. Hancock, H. Paterson, C. J. Marshall, A polybasic domain or palmitoylation is required in addition to the CAAX motif to localize p21ras to the plasma membrane. Cell **63**, 133-139 (1990).
55. O. Rocks et al., An acylation cycle regulates localization and activity of palmitoylated Ras isoforms. Science **307**, 1746-1752 (2005).
56. M. Schmick, A. Kraemer, P. I. Bastiaens, Ras moves to stay in place. Trends in cell biology **25**, 190-197 (2015).
57. J. F. Hancock, R. G. Parton, Ras plasma membrane signalling platforms. The Biochemical journal **389**, 1-11 (2005).
58. S. J. Plowman, C. Muncke, R. G. Parton, J. F. Hancock, H-ras, K-ras, and inner plasma membrane raft proteins operate in nanoclusters with differential dependence on the actin cytoskeleton. Proceedings of the National Academy of Sciences of the United States of America **102**, 15500-15505 (2005).
59. W. C. Lin et al., H-Ras forms dimers on membrane surfaces via a protein-protein interface. Proceedings of the National Academy of Sciences of the United States of America **111**, 2996-3001 (2014).
60. J. T. Groves, R. Parthasarathy, M. B. Forstner, Fluorescence imaging of membrane dynamics. Annual review of biomedical engineering **10**, 311-338 (2008).

61. K. Inouye, S. Mizutani, H. Koide, Y. Kaziro, Formation of the Ras Dimer Is Essential for Raf-1 Activation. Journal of Biological Chemistry **275**, 4 (2000).
62. C. K. Weber, J. R. Slupsky, H. A. Kalmes, U. R. Rapp, Active Ras induces heterodimerization of cRaf and BRaf. Cancer research **61**, 3595-3598 (2001).
63. L. K. Rushworth, A. D. Hindley, E. O'Neill, W. Kolch, Regulation and role of Raf-1/B-Raf heterodimerization. Molecular and cellular biology **26**, 2262-2272 (2006).
64. J. Guldenhaupt et al., N-Ras forms dimers at POPC membranes. Biophysical journal **103**, 1585-1593 (2012).
65. S. Muratcioglu et al., GTP-Dependent K-Ras Dimerization. Structure **23**, 1325-1335 (2015).
66. X. Nan et al., Ras-GTP dimers activate the Mitogen-Activated Protein Kinase (MAPK) pathway. Proceedings of the National Academy of Sciences of the United States of America **112**, 7996-8001 (2015).
67. E. A. Kovrigina, A. R. Galiakhmetov, E. L. Kovrigin, The Ras G Domain Lacks the Intrinsic Propensity to Form Dimers. Biophysical journal **109**, 1000-1008 (2015).
68. M. Holderfield, D. K. Morrison, RAS signaling: Divide and conquer. Nature chemical biology **13**, 7-8 (2016).
69. T. S. Freedman et al., A Ras-induced conformational switch in the Ras activator Son of sevenless. Proceedings of the National Academy of Sciences of the United States of America **103**, 16692-16697 (2006).
70. S. M. Christensen et al., One-way membrane trafficking of SOS in receptor-triggered Ras activation. Nature structural & molecular biology **23**, 838-846 (2016).
71. Y. K. Lee et al., Mechanism of SOS PR-domain autoinhibition revealed by single-molecule assays on native protein from lysate. Nat Commun **8**, 15061 (2017).
72. J. Gureasko et al., Role of the histone domain in the autoinhibition and activation of the Ras activator Son of Sevenless. Proceedings of the National Academy of Sciences of the United States of America **107**, 3430-3435 (2010).
73. G. Bollag, F. McCormick, Regulators and effectors of Ras proteins. Annu Rev Cell Biol **7**, 601-632 (1991).
74. A. E. Karnoub, R. A. Weinberg, Ras oncogenes: split personalities. Nat Rev Mol Cell Bio **9**, 517-531 (2008).
75. Y. Pylayeva-Gupta, E. Grabocka, D. Bar-Sagi, RAS oncogenes: weaving a tumorigenic web. Nat Rev Cancer **11**, 761-774 (2011).
76. J. Omerovic, I. A. Prior, Compartmentalized signalling: Ras proteins and signalling nanoclusters. The FEBS journal **276**, 1817-1825 (2009).
77. D. Abankwa, A. A. Gorfe, J. F. Hancock, Ras nanoclusters: Molecular structure and assembly. Semin Cell Dev Biol **18**, 599-607 (2007).
78. S. Gysin, M. Salt, A. Young, F. McCormick, Therapeutic strategies for targeting ras proteins. Genes & cancer **2**, 359-372 (2011).
79. E. Santos, Dimerization opens new avenues into ras signaling research. Science signaling **7**, pe12 (2014).
80. H. Ledford, Cancer: The Ras renaissance. Nature **520**, 278-280 (2015).
81. J. A. Nye, J. T. Groves, Kinetic control of histidine-tagged protein surface density on supported lipid bilayers. Langmuir : the ACS journal of surfaces and colloids **24**, 4145-4149 (2008).

82. J. Guldenhaupt et al., N-Ras Forms Dimers at POPC Membranes. Biophys J **103**, 1585-1593 (2012).
83. T. S. C. Serena Muratcioglu, Benjamin C. Freed, Hyunbum Jang, Lyuba Khavrutskii, R. Natasha Freed4, Marzena A. Dyba, Karen Stefanisko, Sergey G. Tarasov, Attila Gursoy, Ozlem Keskin, Nadya I. Tarasova, Vadim Gaponenko, Ruth Nussinov GTP-Dependent K-Ras Dimerization. Structure **In Press**, (2015).
84. W. C. Lin et al., H-Ras forms dimers on membrane surfaces via a protein-protein interface. P Natl Acad Sci USA **111**, 2996-3001 (2014).
85. M. J. Davies, Singlet oxygen-mediated damage to proteins and its consequences. Biochemical and biophysical research communications **305**, 761-770 (2003).
86. P. D. Ray, B. W. Huang, Y. Tsuji, Reactive oxygen species (ROS) homeostasis and redox regulation in cellular signaling. Cellular signalling **24**, 981-990 (2012).
87. C. K. Prier, D. A. Rankic, D. W. C. MacMillan, Visible Light Photoredox Catalysis with Transition Metal Complexes: Applications in Organic Synthesis. Chem Rev **113**, 5322-5363 (2013).
88. C. H. Yu, J. T. Groves, Engineering supported membranes for cell biology. Med Biol Eng Comput **48**, 955-963 (2010).
89. J. T. Groves, C. Wulfing, S. G. Boxer, Electrical manipulation of glycan phosphatidyl inositol tethered proteins in planar supported bilayers. Biophys J **71**, 2716-2723 (1996).
90. J. D. Knight, M. G. Lerner, J. G. Marcano-Velazquez, R. W. Pastor, J. J. Falke, Single Molecule Diffusion of Membrane-Bound Proteins: Window into Lipid Contacts and Bilayer Dynamics. Biophys J **99**, 2879-2887 (2010).
91. T. P. A. Devasagayam, A. R. Sundquist, P. Di Mascio, S. Kaiser, H. Sies, Activity of Thiols as Singlet Molecular-Oxygen Quenchers. J Photoch Photobio B **9**, 105-116 (1991).
92. I. Rasnik, S. A. McKinney, T. Ha, Nonblinking and long-lasting single-molecule fluorescence imaging. Nat Methods **3**, 891-893 (2006).
93. A. Wright, W. A. Bubb, C. L. Hawkins, M. J. Davies, Singlet oxygen-mediated protein oxidation: Evidence for the formation of reactive side chain peroxides on Tyrosine residues. Photochem Photobiol **76**, 35-46 (2002).
94. A. Michaeli, J. Feitelson, Reactivity of singlet oxygen toward amino acids and peptides. Photochem Photobiol **59**, 284-289 (1994).
95. V. Kasche, L. Lindqvist, Reactions between Triplet State of Fluorescein + Oxygen. J Phys Chem-Us **68**, 817-& (1964).
96. J. W. Heinecke, W. Li, H. L. Daehnke, J. A. Goldstein, Dityrosine, a Specific Marker of Oxidation, Is Synthesized by the Myeloperoxidase-Hydrogen Peroxide System of Human Neutrophils and Macrophages. J Biol Chem **268**, 4069-4077 (1993).
97. H. R. Shen, J. D. Spikes, C. J. Smith, J. Kopecek, Photodynamic cross-linking of proteins - V. Nature of the tyrosine-tyrosine bonds formed in the FMN-sensitized intermolecular cross-linking of N-acetyl-L-tyrosine. J Photoch Photobio A **133**, 115-122 (2000).
98. D. A. Malencik, S. R. Anderson, Dityrosine as a product of oxidative stress and fluorescent probe. Amino Acids **25**, 233-247 (2003).
99. D. A. Malencik, S. R. Anderson, Dityrosine Formation in Calmodulin. Biochemistry-Us **26**, 695-704 (1987).

100. F. J. Fourniol et al., Micropattern-guided assembly of overlapping pairs of dynamic microtubules. Methods in enzymology **540**, 339-360 (2014).
101. W. C. Lin, C. H. Yu, S. Triffo, J. T. Groves, Supported membrane formation, characterization, functionalization, and patterning for application in biological science and technology. Current protocols in chemical biology **2**, 235-269 (2010).
102. E. F. Pettersen et al., UCSF Chimera--a visualization system for exploratory research and analysis. J Comput Chem **25**, 1605-1612 (2004).
103. M. P. Sheetz, D. E. Koppel, Membrane Damage Caused by Irradiation of Fluorescent Concanavalin-A. P Natl Acad Sci USA **76**, 3314-3317 (1979).
104. J. D. Goosey, J. S. Zigler, J. H. Kinoshita, Cross-Linking of Lens Crystallins in a Photodynamic System - a Process Mediated by Singlet Oxygen. Science **208**, 1278-1280 (1980).
105. T. Niedermayer et al., Intermittent depolymerization of actin filaments is caused by photo-induced dimerization of actin protomers. P Natl Acad Sci USA **109**, 10769-10774 (2012).
106. E. M. Smith, P. J. Macdonald, Y. Chen, J. D. Mueller, Quantifying Protein-Protein Interactions of Peripheral Membrane Proteins by Fluorescence Brightness Analysis. Biophys J **107**, 66-75 (2014).
107. V. J. Thannickal, B. L. Fanburg, Reactive oxygen species in cell signaling. Am J Physiol-Lung C **279**, L1005-L1028 (2000).
108. T. Cordes, J. Vogelsang, P. Tinnefeld, On the mechanism of Trolox as antiblinking and antibleaching reagent. Journal of the American Chemical Society **131**, 5018-5019 (2009).
109. C. E. Aitken, R. A. Marshall, J. D. Puglisi, An oxygen scavenging system for improvement of dye stability in single-molecule fluorescence experiments. Biophysical journal **94**, 1826-1835 (2008).
110. K. Jaqaman et al., Robust single-particle tracking in live-cell time-lapse sequences. Nature methods **5**, 695-702 (2008).
111. C. A. Karlovich et al., In vivo functional analysis of the Ras exchange factor son of sevenless. Science **268**, 576-579 (1995).
112. H. H. Jeng, L. J. Taylor, D. Bar-Sagi, Sos-mediated cross-activation of wild-type Ras by oncogenic Ras is essential for tumorigenesis. Nat Commun **3**, 1168 (2012).
113. N. Li et al., Guanine-nucleotide-releasing factor hSos1 binds to Grb2 and links receptor tyrosine kinases to Ras signalling. Nature **363**, 85-88 (1993).
114. P. Chardin et al., Human Sos1: a guanine nucleotide exchange factor for Ras that binds to GRB2. Science **260**, 1338-1343 (1993).
115. S. E. Egan et al., Association of Sos Ras exchange protein with Grb2 is implicated in tyrosine kinase signal transduction and transformation. Nature **363**, 45-51 (1993).
116. M. Rozakis-Adcock, R. Fernley, J. Wade, T. Pawson, D. Bowtell, The SH2 and SH3 domains of mammalian Grb2 couple the EGF receptor to the Ras activator mSos1. Nature **363**, 83-85 (1993).
117. M. Tartaglia et al., Gain-of-function SOS1 mutations cause a distinctive form of Noonan syndrome. Nat Genet **39**, 75-79 (2007).
118. A. E. Roberts et al., Germline gain-of-function mutations in SOS1 cause Noonan syndrome. Nat Genet **39**, 70-74 (2007).

119. F. Lepri et al., SOS1 mutations in Noonan syndrome: molecular spectrum, structural insights on pathogenic effects, and genotype-phenotype correlations. Hum Mutat **32**, 760-772 (2011).
120. T. C. Hart et al., A mutation in the SOS1 gene causes hereditary gingival fibromatosis type 1. Am J Hum Genet **70**, 943-954 (2002).
121. J. Das et al., Digital signaling and hysteresis characterize ras activation in lymphoid cells. Cell **136**, 337-351 (2009).
122. E. Genot, D. A. Cantrell, Ras regulation and function in lymphocytes. Curr Opin Immunol **12**, 289-294 (2000).
123. J. P. Roose, M. Mollenauer, M. Ho, T. Kurosaki, A. Weiss, Unusual interplay of two types of Ras activators, RasGRP and SOS, establishes sensitive and robust Ras activation in lymphocytes. Molecular and cellular biology **27**, 2732-2745 (2007).
124. R. L. Kortum et al., Targeted Sos1 deletion reveals its critical role in early T-cell development. Proceedings of the National Academy of Sciences of the United States of America **108**, 12407-12412 (2011).
125. K. K. Yadav, D. Bar-Sagi, Allosteric gating of Son of sevenless activity by the histone domain. Proceedings of the National Academy of Sciences of the United States of America **107**, 3436-3440 (2010).
126. B. K. Jaitner et al., Discrimination of amino acids mediating Ras binding from noninteracting residues affecting raf activation by double mutant analysis. The Journal of biological chemistry **272**, 29927-29933 (1997).
127. J. Vogelsang et al., A reducing and oxidizing system minimizes photobleaching and blinking of fluorescent dyes. Angew Chem Int Ed Engl **47**, 5465-5469 (2008).
128. S. Boykevisch et al., Regulation of ras signaling dynamics by Sos-mediated positive feedback. Curr Biol **16**, 2173-2179 (2006).
129. S. L. Campbell, R. Khosravi-Far, K. L. Rossman, G. J. Clark, C. J. Der, Increasing complexity of Ras signaling. Oncogene **17**, 1395-1413 (1998).
130. K. Scheffzek et al., Structural analysis of the GAP-related domain from neurofibromin and its implications. The EMBO journal **17**, 4313-4327 (1998).
131. G. Bollag, F. McCormick, Differential regulation of rasGAP and neurofibromatosis gene product activities. Nature **351**, 576-579 (1991).
132. D. Abankwa, A. A. Gorfe, J. F. Hancock, Ras nanoclusters: molecular structure and assembly. Seminars in cell & developmental biology **18**, 599-607 (2007).
133. L. Janosi, Z. Li, J. F. Hancock, A. A. Gorfe, Organization, dynamics, and segregation of Ras nanoclusters in membrane domains. Proceedings of the National Academy of Sciences of the United States of America **109**, 8097-8102 (2012).
134. G. Zimmermann et al., Small molecule inhibition of the KRAS-PDEdelta interaction impairs oncogenic KRAS signalling. Nature **497**, 638-642 (2013).
135. B. Sperlich, S. Kapoor, H. Waldmann, R. Winter, K. Weise, Regulation of K-Ras4B Membrane Binding by Calmodulin. Biophysical journal **111**, 113-122 (2016).
136. A. Edelstein, N. Amodaj, K. Hoover, R. Vale, N. Stuurman, Computer control of microscopes using microManager. Curr Protoc Mol Biol **Chapter 14**, Unit14 20 (2010).
137. Y. Zhou et al., Lipid-Sorting Specificity Encoded in K-Ras Membrane Anchor Regulates Signal Output. Cell **168**, 239-251 e216 (2017).

138. P. Prakash et al., Computational and biochemical characterization of two partially overlapping interfaces and multiple weak-affinity K-Ras dimers. Sci Rep **7**, 40109 (2017).
139. M. Drosten et al., Genetic analysis of Ras signalling pathways in cell proliferation, migration and survival. The EMBO journal **29**, 1091-1104 (2010).
140. A. E. Aplin, S. A. Stewart, R. K. Assoian, R. L. Juliano, Integrin-mediated adhesion regulates ERK nuclear translocation and phosphorylation of Elk-1. The Journal of cell biology **153**, 273-282 (2001).
141. S. A. McKinney, C. S. Murphy, K. L. Hazelwood, M. W. Davidson, L. L. Looger, A bright and photostable photoconvertible fluorescent protein. Nature methods **6**, 131-133 (2009).
142. N. Mochizuki et al., Spatio-temporal images of growth-factor-induced activation of Ras and Rap1. Nature **411**, 1065-1068 (2001).
143. H. Murakoshi et al., Single-molecule imaging analysis of Ras activation in living cells. Proceedings of the National Academy of Sciences of the United States of America **101**, 7317-7322 (2004).
144. C. D. Harvey, R. Yasuda, H. Zhong, K. Svoboda, The spread of Ras activity triggered by activation of a single dendritic spine. Science **321**, 136-140 (2008).
145. J. E. Toettcher, O. D. Weiner, W. A. Lim, Using optogenetics to interrogate the dynamic control of signal transmission by the Ras/Erk module. Cell **155**, 1422-1434 (2013).
146. E. Nogales, The development of cryo-EM into a mainstream structural biology technique. Nature methods **13**, 24-27 (2016).
147. H. Shankaran et al., Rapid and sustained nuclear-cytoplasmic ERK oscillations induced by epidermal growth factor. Molecular systems biology **5**, 332 (2009).
148. J. G. Albeck, G. B. Mills, J. S. Brugge, Frequency-modulated pulses of ERK activity transmit quantitative proliferation signals. Molecular cell **49**, 249-261 (2013).
149. K. Aoki et al., Stochastic ERK activation induced by noise and cell-to-cell propagation regulates cell density-dependent proliferation. Molecular cell **52**, 529-540 (2013).
150. B. N. Kholodenko, Negative feedback and ultrasensitivity can bring about oscillations in the mitogen-activated protein kinase cascades. Eur J Biochem **267**, 1583-1588 (2000).